A POLARIZATION INSENSITIVE METAMATERIAL ABSORBER FOR THE APPLICATION OF SOLAR ENERGY HARVESTING IN THE OPTICAL REGIME

by

MD HASANUL KARIM

JOHAN UDDIN

BACHELOR OF SCIENCE IN ELECTRICAL AND ELECTRONIC ENGINEERING

Department of Electrical and Electronic Engineering
INTERNATIONAL ISLAMIC UNIVERSITY CHITTAGONG

APRIL 2022

A POLARIZATION INSENSITIVE METAMATERIAL ABSORBER FOR THE APPLICATION OF SOLAR ENERGY HARVESTING IN THE OPTICAL REGIME

by

MD HASANUL KARIM

JOHAN UDDIN

A thesis
submitted as partial fulfilment of the requirement for the degree of

BACHELOR OF SCIENCE IN ELECTRICAL AND ELECTRONIC ENGINEERING

Department of Electrical and Electronic Engineering
INTERNATIONAL ISLAMIC UNIVERSITY CHITTAGONG

APRIL 2022

CERTIFICATE OF APPROVAL

The thesis entitled as "**A polarization insensitive metamaterial absorber for the application of solar energy harvesting in the optical regime**" submitted by **Md Hasanul Karim**, bearing Matric ID. **ET171012** and **Johan Uddin**, bearing Matric ID. **ET171003** of session **Autumn 2020**, to the Department of Electrical and Electronic Engineering, International Islamic University Chittagong, has been accepted as satisfactory in partial fulfilment of the requirements for the degree of Bachelor of Science in Engineering and approved for the examination held on **16 April, 2022**.

_____

Supervisor
Dr. Sikder Sunbeam Islam
Associate Professor,
Department of Electrical and Electronic Engineering,
International Islamic University Chittagong.

DECLARATION

It is hereby declared that this work has been done by us and no portion of the work contained in this thesis has been submitted elsewhere for the award of any degree or diploma.

_____

Md Hasanul Karim

_____

Johan Uddin

ACKNOWLEDGMENT

All praises and thanks to Allah, the Lord of the world, the Most Beneficent, the Most Merciful for helping us to accomplish this work.

Firstly, we would like to express our cordial thanks and gratitude to our supervisor Dr. Sikder Sunbeam Islam who gave us the golden opportunity to do this wonderful research work. This thesis helped us in doing a lot of research and we came to know about so many new things. We are thankful to him.

Secondly, we would also like to thank our parents and seniors who helped us a lot in finalizing this thesis within the limited time frame.

Md Hasanul Karim
Johan Uddin

ABSTRACT

Metamaterial absorbers have sparked a lot of interest due to their significant capacity to achieve nearly perfect absorption in nanostructures. Particularly Metamaterial absorbers can greatly increase the efficiency of solar energy by amplifying the solar electromagnetic wave. Since Solar energy is considered one of the cleanest renewable energy sources, the development of high-efficiency broadband solar absorption devices is essential. Metamaterial absorbers typically operate with a wide absorption band within the visible frequency range for solar energy collection. In this paper, we presented a new type of broadband solar energy absorber based on tungsten (W) to achieve broadband solar energy absorption. This tri-layer meta-absorber is designed by Finite Integration Technique (FIT) using CST microwave studio simulation software. The design shows that the nanostructure has a long absorption band from 400nm to 800nm with average absorption rates of 96.62% and near unity absorbance is achieved at around 604.91 nm. The proposed model has an absorption level of 94.58% on average. The designed MA shows nearly similar absorbance and reflectance in three modes such as transverse electromagnetic (TEM), transverse electric (TE), and transverse magnetic (TM). The suggested design's absorption efficiency data are also compared with previously published similar absorber designs to demonstrate the improvement of absorption in the proposed design. These results show significant possibilities to enrich integrated terahertz devices and many other practical applications like sensor and thermophotovoltaic cells.

TABLE OF CONTENTS

LIST OF FIGURES

LIST OF TABLES

LIST OF ABBREVIATIONS

CST MWS	Computer Simulation Technology Microwave Studio
CST	Computer Simulation Technology
EM	Electromagnetic
FBW	Fractional Bandwidth
FIT	Finite Integration Technique
FSS	Frequency Selective Surface
HAADF	High Angle Annular Dark Field
MMA	Metamaterial Absorber
PEC	Perfect Electric Conductor
PEMC	Perfect Electromagnetic Conductor
PMA	Perfect Metamaterial Absorber
PMC	Perfect Magnetic Conductor
PML	Perfectly Matched Layer
STEM	Scanning Transmission Electron Microscopy
STPV	Solar Thermophotovoltaics
TE	Transverse Electric
TEM	Transverse Electromagnetic
TM	Transverse Magnetic
SAR	Specific Absorption Rate
RCS	Radio Cross Section
MMA	Metamaterial Absorber
ZIM	Zero Index Metamaterial
DNG	Double Negative Metamaterial
NIM	Negative Index Materials
LHM	Left-Handed Materials
BWM	Backward Wave Media

CHAPTER 1
INTRODUCTION

1.1 Introduction

1.1.1 Energy Challenge

Energy is a necessary component of human life. It is required to create and distribute our food, to keep us cold or warm, to provide clean water, to assist us in our daily activities, and to manufacture the things on which we rely. There is no industrial, medical, agricultural or household process that does not utilize some type of external energy. Growing global energy demand as well as issues of scarcity and environmental effects linked with traditional energy sources are bringing the entire world on the verge of an energy disaster within the next two or three decades. Petroleum will become more limited and expensive and the widespread use of all fossil fuels will increase the climatic effect. At the same time, present nuclear power plants will have reached the end of their useful life. Because existing power sources cannot be eliminated, they must be adjusted to eliminate or reduce environmental pollution and new sources, especially renewable sources must be added. Here one of the best alternative energy sources would be Solar Energy.

1.1.2 Clean Energy Demand

The path is not so far when rising energy consumption will push us to look for environmentally friendly alternative energy sources. The majority of our electricity is generated by coal, gas, nuclear, and other non-renewable energy sources. The production of energy from these resources has a tremendous detrimental influence on our ecosystem, damaging our land, air, and water in many ways. The production of electricity releases more greenhouse emissions than all of our driving and flying combined. In word Fossil fuels are the largest driver of climate change and are still our primary source of energy. On the other hand, clean energy eliminates toxic smog, toxic poisonous compounds in our air and water, and the effects of coal mining and gas extraction. As a result, substantial renewable energy implementation plans must incorporate techniques for integrating renewable sources into coherent energy networks impacted by energy savings and efficiency measures. Nanomaterials' introduction as new building blocks for light energy harvesting systems has opened up a new dimension for utilizing renewable energy sources.

1.1.3 Solar Energy

Solar energy is any type of energy generated by sunlight. Nuclear fusion happens in the sun, resulting in solar energy. Protons from hydrogen atoms fuse to generate helium atoms when they collide strongly in the sun's core. Photovoltaic cell receives solar radiation produces heat, causes chemical reactions, or generate electricity. The entire amount of solar energy incident on Earth is sufficient to meet the world's energy needs every day. This source of energy has the capacity to solve all of the world's future energy demands. For this, solar cell for power generation is getting a lot of popularity these days, not least from the general public. Solar energy is still more expensive than conventionally generated electricity. On the other hand, solar electricity will undoubtedly play an important part in off-grid situations and building components that provide unique and desired architectural expressions. It will create many new jobs and employments, save our eco-system and livelihood. It is sustainable and it has lower maintenance. Above all, this is the ultimate energy solution for a green environment. Thus far, it seems that solar energy will be the best alternative energy source for the world's present energy challenge.

1.1.4 Metamaterial

Meta is a Greek word that means "beyond". This word is a combo of "meta" and "material." The electromagnetic properties of metamaterials can be changed to something that isn't found in nature. Metamaterials are novel artificial materials with unique electromagnetic properties not seen in natural materials. Even though all natural materials have a positive electrical permittivity, the new artificially constructed materials are known as negative index materials (NIM), double-negative (DNG) media, left-handed (LH) materials or backward wave (BW) media all have negative electrical permittivity. These properties can be made from their precise shape, geometry, size, orientation, and arrangement by nanofabrication. Hence manipulation of electromagnetic waves can be possible by absorbing, blocking, amplifying, or bending waves to obtain maximum benefits that are not attainable with ordinary materials. From these unusual material parameters, new kinds of nanoscale antennas and microwave modules such as solar absorbers, thermal emitters etc can be created for domestic or industrial purposes especially in wireless communications defence industries.

1.1.5 Field of Metamaterial

- Energy harvesting
- Waveguide Design
- Filter Design
- Antenna Design
- Absorber Design
- Invisibility Cloak Design
- Sensing as Sensor
- Solar Cell Design
- Thermal imaging
- SAR and RCS Reduction
- Wireless Power Transfer
- Photovoltaics
- EM interference shielding
- Magnetic imaging
- Thermal emitters
- Optical Modulator
- Light Trapper

1.1.6 Metamaterial Absorber to Utilize Solar Energy

Artificial materials are known as metamaterials. They are made up many different types of composite materials including metals and polymers. They are rarely found in nature. They possess incredible electromagnetic characteristics. These characteristics can be used to create effective solar absorbers. We know that the usual absorber has a very low absorption. The use of metamaterial for solar absorbers can help to overcome this low efficiency. Solar absorbers made with metamaterials are significantly more efficient than traditional absorbers. Because these can absorb about whole visible and infrared spectrum. Metamaterial absorbers have been the subject of numerous studies. In this research, we're also looking for a perfect metamaterial absorber of this type.

1.2 Literature Review

Due to an ambient source of renewable energy, solar energy harvesting has created a great interest among researchers by nanostructure building block[1]–[4]. Having an exotic property of metamaterial to absorb optical wavelength many efficient absorbers were designed after Landy (2008)[5], [6]. Before this Physicist Victor Veselgo (1967) explained the dielectric properties of a matter that generally does not show the characteristics of natural material; as the values of permittivity and permeability are negative[7]. Smith et al (2004) developed a gradient refractive index medium to distort electromagnetic waves based on this approach[8]. After that, metamaterial research got a new dimension in the engineering field and scientific communities due to their unique capacity to challenge the limits of regular materials and give remarkable properties[9]. Today Metamaterial absorber (MA) is manipulated in various field in material engineering such as antenna[10]–[12], superlens[13]–[16], absorber[17], phase compensator[18], emitter[19], filter[20], [21], invisible cloaking[22]–[24], magnetic resonance imaging (MRI)[25], [26], detector[27], waveguide[28]–[31], SAR[32], thermal imaging[33]–[35], energy harvesting[36], wide-angle stability[37] and different type of sensor[38]–[40]. In general, an MA resembles a sandwiched structure in which two patterned metallic layers are separated by a dielectric material and whose absorption spectra are mostly dictated by layer patterns and parameter combinations[41]–[43]. The electromagnetic (EM) wave is blocked by the metal layer, and the dielectric layer assists the structure in creating a coupling capacitance with the metal layer[44], [45]. Nevertheless, these are not the only factors that contribute to a near-perfect MMA match. Strong field resonance of substrate[46], a good surface charge density along with E-field and H-field[47], the high thickness of bottom layer[48], perfect impedance match of solar wavelength[49], surface plasmon resonance (LSPR)[50], the similarity of free space impedance and meta-surface impedance are also caused higher absorption and lower transmission[51]. Though the most popular version is a three-layer stack, MMA also contains two-layer[52], [53], four-layer[54], [55], and multi-layer stacks[56]–[58]. Despite being ultrathin[59]–[61] and polarization insensitive[62], [63] PMAs have high absorption capacity over a wide wavelength range due to their periodic structure. Today many broadband MMA is proposed for optical spectrum for their popularity. Some of them are detailed here, along with the findings of the investigations, the materials utilized, and the angular and polarizing stability of the materials.

F. Qin et al. suggested a Hexa layer TiN nanodisk and Ti thin film Ultra-broadband nanostructure. This wide-angle perfect solar absorber can operate in wavelength from 300

~ 3000 nm for thermal emitters applications [64]. An ultrathin silicon nanostructure is suggested by Weiren Zhu that has 80% of absorptivity at the spectral region from 437.9 nm to 578.3 nm wavelength. This try layer substrate formed as Si-SiO_2-Au to get peak absorptivity at 567.1 to 647.9 nm about 96% within incident angles 0 to 40◦ [65]. A Broadband response nanostructured new ZIM absorber is introduced by using tungsten and quartz. This try layer shaped unit cell structure with 500 × 500 nm^2 dimensions shows about 89.71% absorptivity in 450-600 nm visible wavelength [66]. Patrick Rufangura proposed a try layer nanostructure to enhance the efficiency of PV cells. The designed MTM absorber shows two absorption peaks nearly unity absorption at 543.75 THz and 663.75 both TE and TM polarization angles [67]. A new ultra-thin solar absorber has been introduced by M. H. Heidari for minimizing cell size and maximizing the bandwidth. The matrix notated Cu-Au based design has dimensions 320 × 320 nm^2 Containing about 90% absorption [68]. A plasmonic broadband absorber offered by P. Zhu to enhance photovoltaics and thermal emitters devices. This dual grating MMA has nearly 80% absorption from 400 nm to 600 nm wavelength where the unit cell structure was Cu/Si3N4/Cu [69]. The numerical study of a broadband MA was proposed by Tran Sy Tuan in the visible light spectrum with some infrared regions where absorptivity exceeded 90% for both TE and TM polarizations for visible light applications[70]. M.A. Baqir designed a three-layer U-shaped nanostructure of gold, silica and copper. Peak absorption of about 99% was found in aforesaid spectral range both TE and TM polarization mode to work as heat-absorbing media and solar cell [71]. An efficient absorber designed by Phuc Toan Dang exhibits 98% absorption at a large wideband range of 417–1091 nm where absorption stability is almost 95% at optimum incident angles up to 40 [72]. Nguyen et all investigated a multi-layered conical frustums absorber that indicated an absorptivity of more than 90%, which covered the full visible and near-infrared region up to 60° incident angles [73]. MMA have been shown in various spectral range to date, including radiowave[74], microwave[75], mm-Wave[76], THz[77], MIR[78], NIR[79], IR[80], UV[81] to the near optical[82]. Moreover, metamaterial was used in many applications such as cryptography[83], light trapper[84], reflector[85], sound absorption[86], thermal detector[87], photonic circuit[88], military radar devices[89], RFID systems[90], detection of explosives[91], STPV[92], refractive index sensor[93], glucose[94] and ethanol[95] sensor, underwater sound absorption[96].

1.3 Research Goal

Propelled by earlier work with various applications in the related field, an MMA is introduced here for the whole optical region. From the previous literature review, it can be observed that an MMA with an average absorption of up to 95% is not highly accessible for TE and TM mode with a larger than 60° incidence angle. To improve this limitation a simple try layer nanostructured double negative (DNG) metamaterial absorber has been proposed from 400nm to 800nm with a broadband absorption using Tungsten (optical) and Silicon dioxide (optical) as metal and dielectric respectively. This design includes a ring with a plus sign as its top layer. Wave is primarily absorbed here. Our main purpose is to improve the absorbance at the visible frequency range because it has great importance in energy harvesting. The absorbance crest of our proposed nanostructure is better than many other proposed metamaterials unit cells. Our proposed design structure is very simple and flexible so that it can be easily possible for industrial implementation. The Result of this design proves that the nanostructure has a long absorption band from 400nm to 800nm with average absorption rates of 96.62% that are included in the visible region. The proposed model has an absorption level of 91.20% all the time. This MMA shows almost perfect absorption of 99.99% at 604.91 nm and over 99% absorption from 535 to 682nm. The designed MA shows nearly similar absorbance and reflectance in three modes such as transverse electromagnetic (TEM), transverse electric (TE), and transverse magnetic (TM). The physical origin of this design is investigated by analyzing their field distributions. The insensitivity of polarization angle has also been verified. To find the best absorbance and reflectance of the MMA, the shape and parameters were changed frequently of the structure. To analyze the numerical calculations of the absorbance and reflectance from scattering parameters FIT is used in CST MWS software and the numerical analysis is verified in MATLAB.

1.4 Organization of the paper

- Chapter 1 Introduction: This chapter discusses solar energy and the present state of the world's energy. Previous works on metamaterial absorbers are also included in chronological order. A summary of the research goal is also included.

- Chapter 2 Design & Simulation: The design steps are properly discussed in this chapter. The design of the substrate and resonator, as well as their parameters, are given. The suitable boundary condition selection and simulation setup are briefly presented.

- Chapter 3 Result Analysis: For accurate characterization of the PMA absorber, extensive parametric inspections were performed. Individual peaks are analysed using the Scattering parameter. The qualities of an effective medium are investigated. The model's Fairfield and mesh views are also mentioned. This chapter compares the model to various previous works like this in respect of bandwidth, materials, polarization angle and absorption

- Chapter 4 Conclusion: The chapter provides a quick overview of the work completed as well as the possibility of future projects.

CHAPTER 2
DESIGN & SIMULATION

2.1 Introduction

This study is based on a simulation created with CST Studio which includes the FIT technique. This type of nanoscale metamaterial research has yet to be put into practical practice. Some techniques were taken to simulate our proposed concept in CST. The material selection, design, and simulation processes are all addressed in depth in this chapter.

2.2 Choice of Material

Since the suggested metamaterial design operates in the optical frequency, we must choose metal and dielectric layers that are stable at high temperatures and have ideal optical properties. Various types of Materials can be used to construct the required building model. We studied the qualities of many materials and concluded that Tungsten and Silicon dioxide provided the greatest results. So, our structure will be W-SiO_2-W three-layered structure.

2.2.1 Tungsten

In recent years, high-loss metallic materials and dielectric materials with a short bandgap have been popular choices for constructing absorbers[97]. Tungsten has a high intrinsic loss, resulting in essentially no propagation through the ground slab and reduced reflection across the unit cell[98]. Having a good impedance match in free space and low ohmic loss Tungsten is good choice for selecting as resonator and ground layer. The physical structure is critical for detecting the resonance wavelength. These resonance qualities are mostly attributable to the loss of electromagnetic wave energy by the absorber's electromagnetic resonance mode and the field dissipation effect generated by the tungsten metal layer's high imaginary[59]. Raw Tungsten metal and its scanning transmission electron microscopic annular dark-field imaging have been shown in **Fig. 2.1** and the properties are listed in **Table 2.1.**

(a)

(b)

Fig. 2.1 (a) Raw Tungsten Metal (b) SEM micrograph of the virgin microstructure of the Tungsten surface

Table 2.1 Properties of Tungsten (Optical) from CST Library**

Component 1: Top layer and Bottom layer	
Material	Tungsten (Optical)
Type	Optical
Mu	1
Electric condition	1.89e+07 [S/m]
Rho	19250 [kg/m^3]
Thermal condition	173 [W/K/m]
Heat capacity	0.134 [kJ/K/kg]
Diffusivity	6.70673e-5 [m^2/s]
Young's modulus	411 [kN/mm^2]
Poisson's ratio	0.28
Thermal expansion	4.5 [1e-6/K]

2.2.2 Silicon Dioxide

Silicon dioxide (SiO_2) is the most popular and frequently used one compound in nanotechnology. It found as the basis element in numerous minerals and construction materials, including glass, brick, and concrete and makes up about 90% of the Earth's crust. Silicon is used to make more than 99 percent of all nanostructure and semiconductor devices. It is used as primary insulator in silicon devices. In recent years, the use of Silicon Dioxide in solar energy harvesting has increased dramatically. Other optoelectronic devices, such as light-emitting diodes and lasers etc. are made from it. For various reasons, SiO_2 is best suited to construct multijunction and high-efficiency solar cells. Such as,

1. SiO_2 layers can be produced thermally on silicon or deposited on a variety of substrates.
2. SiO_2 has such a high absorptivity that it only takes a few millimeters thick cell to absorb sunlight. (Crystalline silicon necessitates a layer thickness of 100 microns or greater.)
3. SiO_2 cells, unlike silicon cells are relatively heat resistant. (Cell temperatures are frequently fairly high, particularly in concentrator applications.)
4. SiO_2 is an excellent insulator with a high dielectric strength and wide band gap.

5. SiO_2 is very resistant to radiation damage. This, along with its high efficiency, makes SiO_2 very desirable for space applications.
6. The interface that forms between silicon and SiO_2 has very few mechanical or electrical defects and is stable over time.

One of the most significant advantages of Silicon Dioxide and its alloys as PV cell materials is the variety of design possibilities available. A SiO_2 base cell can contain numerous layers of slightly varied compositions, allowing the cell designer to accurately control the creation and collection of electrons and holes. (To achieve the same result, silicon cells have been confined to varying the level of doping.) With this level of control, cell designers can gradually increase efficiency to theoretical levels. In example, one of the most frequent SiO_2 cell designs employs a very thin window layer of Tungsten and Silicon dioxide. This thin layer enables the formation of electrons and holes near to the electric field at the junction.

Pyrogenic silica (also known as fumed silica or silica fume) is a very thin colloidal or particulate form of silicon dioxide. It is made by burning $SiCl_4$ in an oxygen-rich hydrocarbon flame to produce SiO_2 "smoke.". The optical properties derived from CST Material Library are listed in **Table 2.2.**

Fig. 2.2 Silica fume

Table 2.2 Properties of Silicon Dioxide (Optical) from CST Library**

Component 2: Middle layer	
Material	Silicon Dioxide (SiO_2)
Type	Optical
Epsilon	11.9
Mu	1
Density	2.27/2.18 g/cm^{-3}
Relative Dielectric Constant	3.7 - 3.9
Thermal conductivity	3.2 x 10^{-3} W/(cm.K)
Dielectric strength	10^7 V/cm
Diffusivity	3.07587e^{-05} [m^2/s]
Young's modulus	6.6 x 10^{10} N/m^2
Poisson's ratio	0.17
Thermal expansion	5.6 [1e^{-7}/K]

2.3 Design Process

Our suggested model is a three-layered sandwiched model where metal array like W-SiO_2-W. Here SiO_2 is the dielectric layer. This W is the top and bottom levels of the model. There is a Plus sign and ring in front of the substrate consisting with W.

2.3.1 Substrate Design

Here Silicon Dioxide acts as the substrate. Silicon Dioxide is the most widely utilized efficient semiconductor which is found in various types of optoelectronic devices. We can use a variety of design configurations on a SiO2 substrate to achieve our expected results. Maintaining the efficiency of the cell largely depends on the design and depth of the layer. In this study we proposed a square-shaped model. By using square-shaped substrate with different thicknesses, different results can be achieved with different significances. After several trials, the best absorption rate is obtained at 300×300 nm^2 size and 160 nm thickness.

2.3.2 Resonator Design

Another important aspect of this modelling is the layout of the Tungsten resonator. We know that when a substance interacts with wavelengths higher than its size, it exhibits strange properties and transforms into a metamaterial. The designed resonator has a plus sign and a ring outside of this sign. The visible light wavelength range is 380 nm to 750

nm. As a result, the resonator is created in such a way that the visible wavelength is larger than the edge wavelength. Because of the ring shape types, the resonator became polarization insensitive. The thickness of the resonator is chosen at 40 nm and it also has a significant effect on the absorption rate. The unit cell and its Front, left view and design steps are shown in **Fig. 2.3, Fig. 2.4, Fig. 2.5** and **Fig. 2.6** respectively.

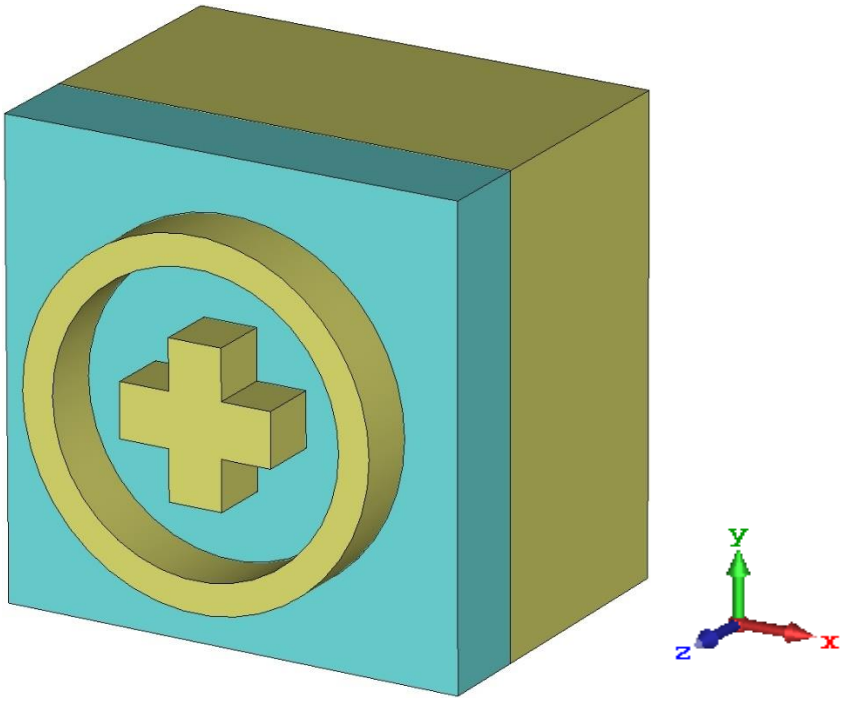

Fig. 2.3 3D view of Metamaterial Absorber Unit cell

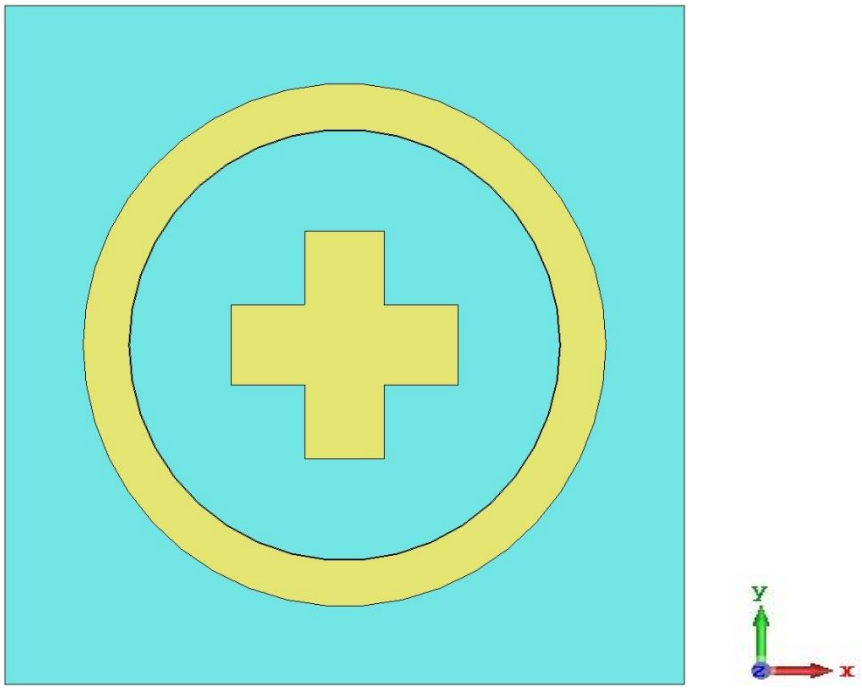

Fig. 2.4 Front view of the unit cell

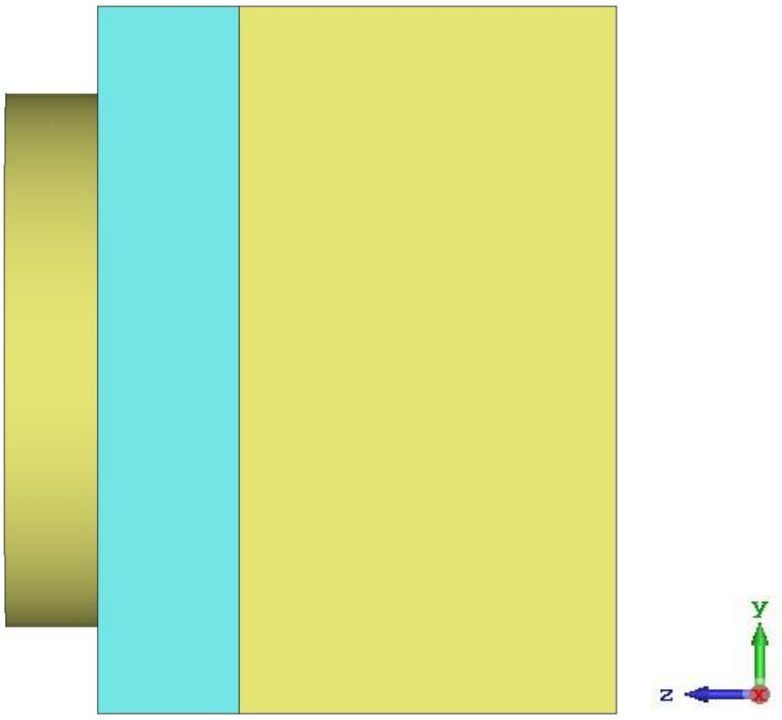

Fig. 2.5 Left side view of the unit cell

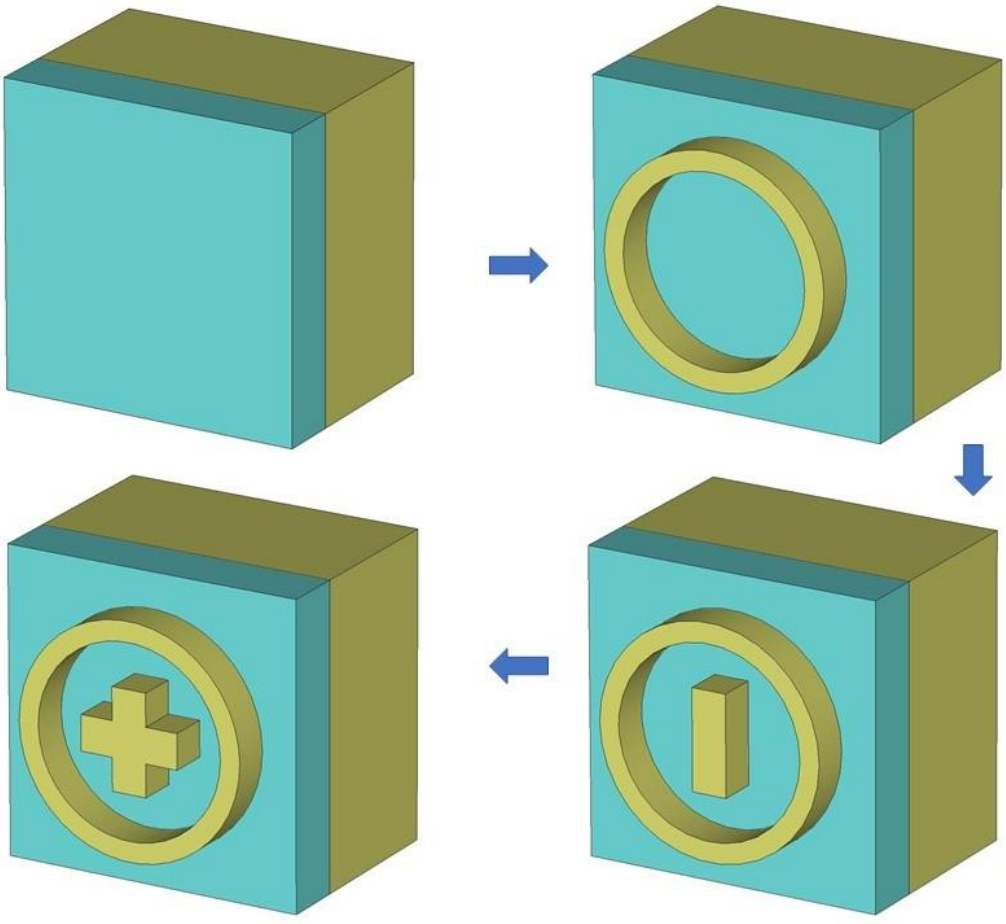

Fig. 2.6 Design steps of the proposed unit cell.

2.3.3 Parameters

The dimensions and all parametric values are depicted in **Fig. 2.7** and tabulated in **Table 2.3**

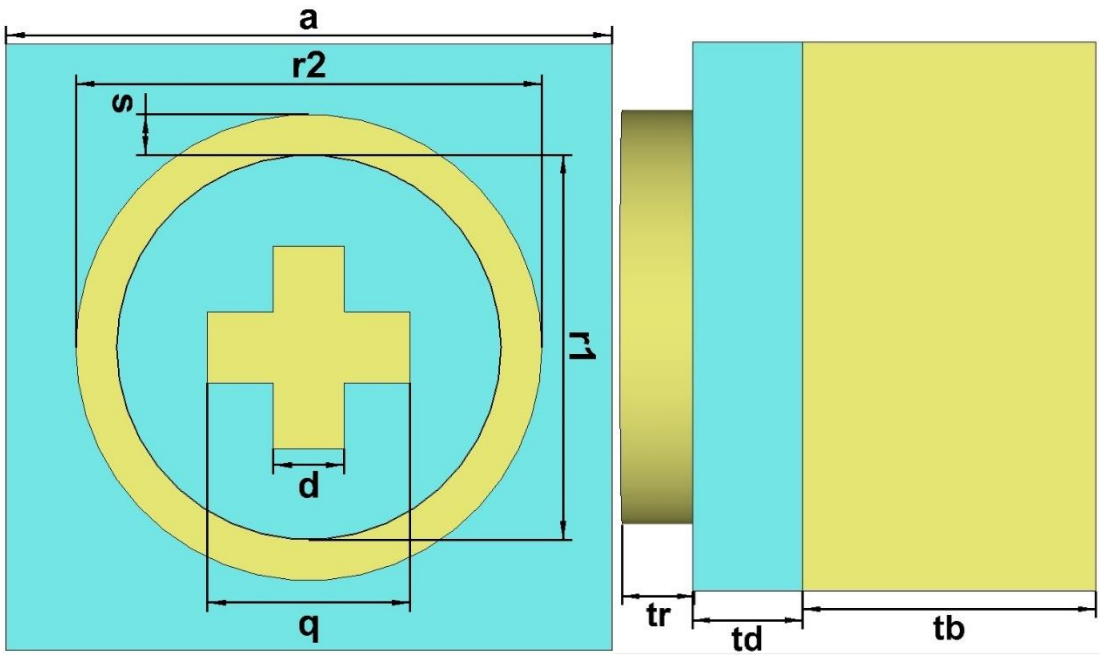

Fig. 2.7 Front and side view with the physical dimension of parameters

Table 2.3 Parameters of proposed PMA structure

Parameters	Value (nm)	Parameters	Value (nm)
Substrate Width, a	300	**Dielectric Thickness, td**	60
Substrate Length, a	300	**Top-level thickness, tr**	40
Plus sign Length, q	100	**Outer Radius, r_2**	115
Ground Plane Thickness,tb	160	**Inner Radius, r_1**	95
Plus sign Width, d	40	**Ring thickness, s**	20

2.3.4 Boundaries

A suitable boundary condition for simulating the model is important since it influences computation stability as well as the system's numerical convergence. The waveguide boundary conditions for TM, TE, and TEM modes have been selected in such a way that the absorber can be used to produce a highly efficient solar cell. The most popular boundary conditions are perfect electric conductor (PEC), perfect magnetic conductor (PMC) and perfect electromagnetic conductor (PEMC). The magnetic field is

asymmetrical and the electric field is symmetrical for the PMC, while the magnetic field is symmetrical and the electric field is asymmetrical for the PEC. The PEMC boundary condition is a nonreciprocal generalization of the PEC and PMC boundary conditions.

PEC : $n \times \mathbf{E} = 0$ and $n.\ \mathbf{B} = 0$

PMC : $n \times H = 0$ and $n.\ \mathbf{D} = 0$

PEMC : $n \times (H + M\mathbf{E}) = 0$ and $n.\ (\mathbf{D} - M\boldsymbol{B}) = 0$

Here, M refers admittance. PEMC was chosen as an appropriate boundary condition because any given PEMC boundary can be transformed into PEC and PMC boundaries. The duality transformation is beneficial when analysing micro scatterers and modelling mixtures including PEMC particles embedded in a background medium with a PEMC boundary. When a PEMC boundary object is placed in an electromagnetic field, the cross-coupling effect of the boundary condition produces a more complex scattering response than when pure dielectric, PEC, or PMC objects are used. Once the electromagnetic response of small PEMC spheres is determined, the effective material parameters of a mixture including such spheres (of subwavelength size) embedded in neutral dielectric background material may be computed.

2.4 Simulation Setup

To obtain the desired absorption rate, a suitable simulation setup and proper boundary conditions are required. The scattering parameter is used to calculate the absorption rate. Some approaches relevant to electromagnetic quantities are suppressed by boundary condition. The periodic boundary condition of the perfect electric conductor (PEC) was taken from the x-axis in this design for the transverse electromagnetic (TEM) mode, while the periodic boundary condition of the perfect magnetic conductor (PMC) was taken from the y-axis. To pass the operational wavelength, a waveguide port is formed in the negative z-axis. To reduce scattering, open space on both sides of the z-axis with a perfectly matched layer (PML) is used. Linearly polarized planar wide-spectrum wave incidence on the top surface of the designed absorber for simulation. The model was simulated in TM and TE mode using a floquet port on the z-axis, with the master and slave on the x- and y-axes, respectively. A higher mesh order is employed to generate more exact simulation results. To simulate the model based on the Finite Integration Technique (FIT), the frequency-domain solver in Computer Simulation Technology Microwave Studio (CST MWS) is used. It is also possible to simulate such metamaterial

absorber models using a time-domain solver. However, the frequency domain solver is more suited to the designed system. To resolve the identical problem, the two solutions employ two distinct approaches. Both solvers are based on the Finite Integration Technique (FIT) and work on the Integral Formulation of Maxwell Equations. Hence it is important that both solvers produce roughly the same results. Both solvers produce identical results if the model is correct and the simulation parameters are properly defined. For smaller structures such as unit cells and FSS-Frequency Selective Surface, frequency domain solutions are effective. A frequency-domain solver can be used to do floquet analysis. Depending on the transient behaviour of the source of excitation and modes, the frequency-domain solution also consumes less time and data than others. When employing time-domain in CST waveguide-ports must be parallel to either the X, Y, or Z axes. In the frequency domain, the waveguide port can have any direction. The mesh is formed in the time domain along the X, Y, and Z axes and makes many small blocks like cubes. To analyse those blocks, harmonic equations in differential or integral form might be used. Finite element technique (FEM) is utilized in the frequency domain to fragment the surface into little triangular objects and integral equations in phasor form are applied for those small surfaces. As a result, the time domain solver works well for wideband structures and the frequency domain solver works well for curved structures.

CHAPTER 3

RESULTS AND DISCUSSION

3.1 Introduction

The simulated results of the designed unit cell that we achieved using CST microwave studio software are analysed in this chapter. Methodology, absorption and reflectance analysis, S parameters, polarization conversion ratio (PCR), polarization angle observation, E field, H field, and surface current are all covered in this chapter. In this chapter, we also analysed the absorption efficiency of this unit cell by changing the various parameters like dielectric and resonator thickness, the diameter of the ring resonator, dielectric material, and resonator material.

3.2 Methodology

The Nicolson-Ross-weir (NRW) method[99] is used to eliminate the S parameter for the estimation of absorption. The Impedance match is so essential for absorbance, the unit cell's impedance and the characteristic impedance

$$Z(\omega) = [\{\mu_r(\omega).\mu_o\}/\{\varepsilon_r(\omega).\varepsilon_o\}]^{1/2} \quad (1)$$

$$Z_0 = (\mu_o/\varepsilon_r)^{1/2} = 377\Omega. \quad (2)$$

Where μ_o denotes free space permeability, ε_o denotes free space permittivity, μ_r denotes relative permeability, and ε_r denotes relative permittivity. Condition ($Z(\omega) = Z_o$) may be accomplished by calibrating the physical dimensions of the design, and the design will give almost unity absorption at a wavelength, which is highly dependent on wavelength. Here, $Z(\omega)$ and Z_o are quite close to the required value; if the values can be equalled, the design might be used as a super absorber with unity absorption. The absorption will be,

$$\begin{aligned} A(\omega) &= 1 - T(\omega) - R(\omega) \\ &= 1 - |S_{21}(\omega)|^2 - |S_{11}(\omega)|^2 \end{aligned} \quad (3)$$

$R(\omega)$ denotes the linear value of the S-parameter (S_{11}), also known as the reflection coefficient, and $T(\omega)$ denotes the linear value of the S_{21} parameter, also known as the transmission coefficient. $T(\omega)$ can be rewritten as near zero due to the large thickness of tungsten, which blocks practically all EM radiation. So the ultimate absorption will be,

$$\begin{aligned} A(\omega) &= 1 - R(\omega) \\ &= 1 - |S_{11}(\omega)|^2 \end{aligned} \quad (4)$$

3.3 Absorption and Reflectance

Fig. 3.1 displays the absorption and reflectance characteristics for transverse electromagnetic (TEM), transverse electric (TE), and transverse magnetic (TM) from 400nm to 800nm, with tungsten as the resonator and silicon dioxide as the dielectric layer. These characteristics are obtained from equations (1) and (2) by using the s-parameter acquired from the simulation. In the optical region, this design has excellent absorption and reflectance for all three modes. Average absorption for TEM, TE, and TM modes are nearly the same. So the design is a good symmetrical design. The average absorption of this unit cell is 96.6% at the optical wavelength range. At 604.91nm, there is a near-unity peak absorption (99.99%) for both three modes. The designed absorber has a day-integrated solar energy absorption of up to 96.6%, which is superior than loss-induced semiconductor absorbers.

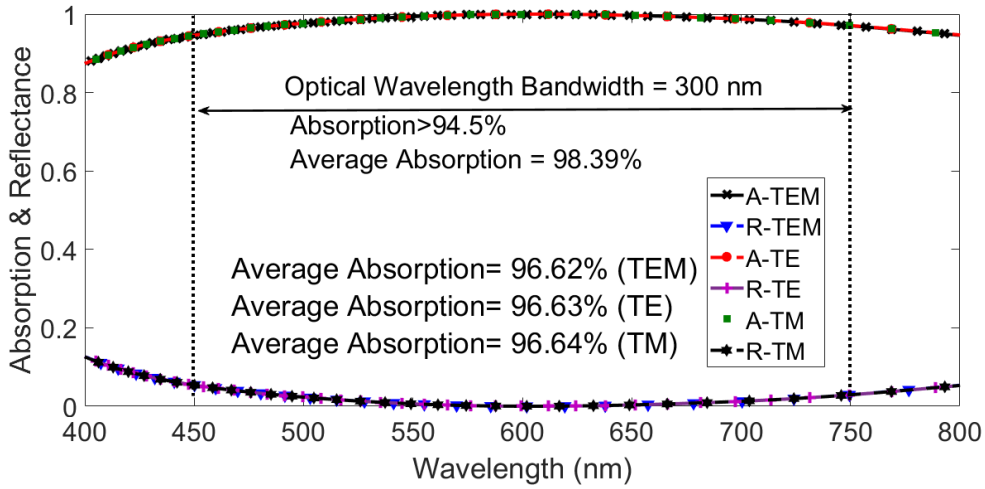

Fig. 3.1 Absorption and Reflectance curve of the design in TEM, TE, and TM mode.

3.4 Co-polarization and cross-polarization with the polarization conversion ratio

As seen above, the absorption curve is executed from (1) and (2). However, with an MMA, one question remains that the unit cell act as a polarization converter and yields the PCR value instead of the absorption. Although the structure is symmetrical, we used (3) and (4) to exhibit both co-polarization and cross-polarization components in **Fig. 3.2**. The cross-polarization component in the linear magnitude scale is almost negligible in **Fig. 3.2**, indicating that the design did not transform the waves in the wave-length region under consideration.

$$|S_{11}(\omega)|^2 = |S_{TE,TE}(\omega)|^2 + |S_{TE,TM}(\omega)|^2$$
$$= R^2_{yy} + R^2_{yx} \quad (5)$$

$$|S_{11}(\omega)|^2 = |S_{TM,TM}(\omega)|^2 + |S_{TM,TE}(\omega)|^2$$
$$= R^2_{xx}R^2_{xy} \quad (6)$$

In this case, $|S_{TE,TE}(\omega)|^2 = |S_{TM,TE}(\omega)|^2 = R_{yy} = R_{xx}$ = co-polarization reflectivity and $|S_{TE,TM}(\omega)|^2 = |S_{TM,TE}(\omega)|^2 = R_{yx} = R_{xy}$ = cross-polarization reflectivity. Furthermore, the PCR of the cell can be computed using (5) or (6), as shown in **Fig 3.3**. The suggested design's PCR value is near zero in both TE and TM mode, which completely removes the issue of polarization conversion characteristics.

$$PCR_{TE} = R^2_{yx} / (R^2_{yy} + R^2_{yx}) \quad (7)$$

$$PCR_{TM} = R^2_{xy} / (R^2_{xx} + R^2_{xy}) \quad (8)$$

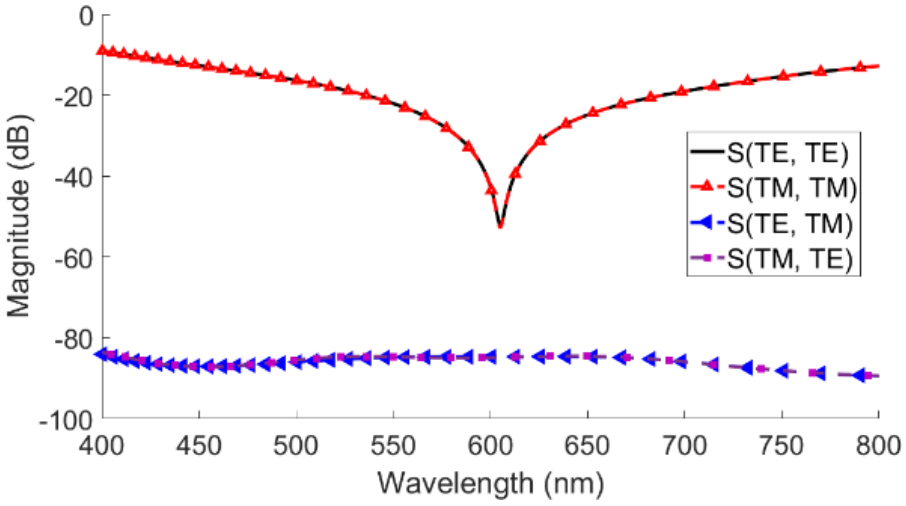

Fig. 3.2 Co-polarization and cross-polarization magnitude (dB) of the reflection coefficient (S_{11}) in the visible region for both TE and TM polarization modes

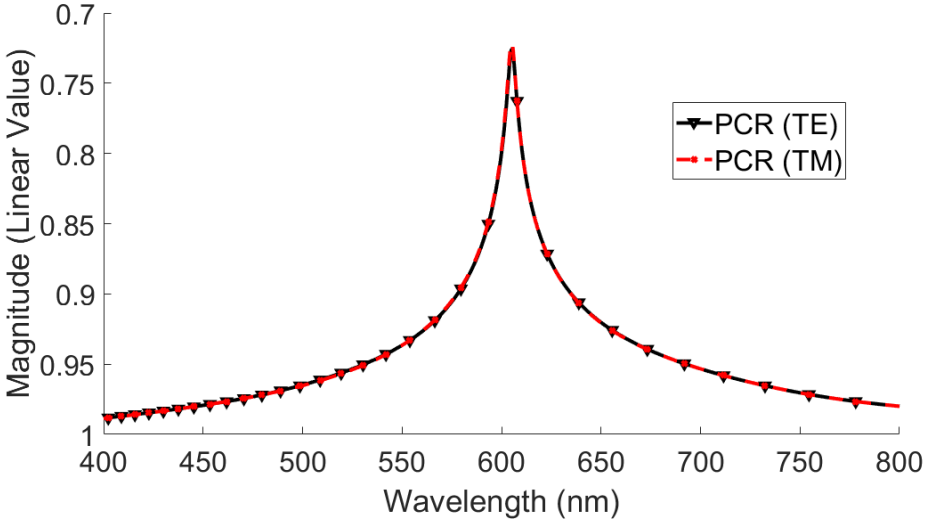

Fig. 3.3 Polarization conversion ratio (PCR) of the designed unit cell in both TE and TM modes.

3.5 Geometric Parameter Analysis

The parameters have a big impact on geometric shape, and the geometric structure has a big impact on absorption. The most essential parameter sweep, as shown in **Fig. 3.4**, **Fig. 3.5**, and **Fig. 3.6** has been explained. A major fluctuation was evident at the change of dielectric thickness (td) as shown in **Fig. 3.4**. A significant change in absorbance has been detected after changing the thicknesses from 50 to 70 nm, and the resonance wavelength has also shifted significantly. Resonance values of 99.90%, 99.98%, 99.99%, 99.96%, and 99.87% were found for dielectric layer thicknesses of 50,55,60,65, and 70 nm, respectively. The resonance wavelengths were linearly changed by dielectric layer thickness at 524, 564, 604.91, 645, and 683 nm, respectively. The resonator thickness (tr) is swept from 30 to 50 nm with a 5 nm increment, and the results are shown in **Fig. 3.4**. The resonance absorption increases as the thickness increases until it reaches 40nm, after which it decreases as the thickness increases. This is because the resonator thickness has an impact on the free space impedance matching. The structure is developed at a thickness of 40nm, which is the best impedance matching. For different "tr" values such as 30, 35, 40, 45, and 50nm, the resonance absorption is 99.86%, 99.96%, 99.99%, 99.98%, and 99.94% respectively. The resonator ring width (s) is swept from 10 to 30 nm with a 5 nm increment, and the results are shown in **Fig. 3.5**. The resonance absorption increases with increasing the resonator ring width until it reaches 20 nm and the resonance absorption decreases when the ring width is more than 20 nm. So, 20 nm ring width is the best for this absorber. For different "s" values such as 10nm, 15nm, 20nm, 25nm, and 30nm, the resonance absorption is 98.11%, 99.53%, 99.99%, 99.63% and 98.74% respectively.

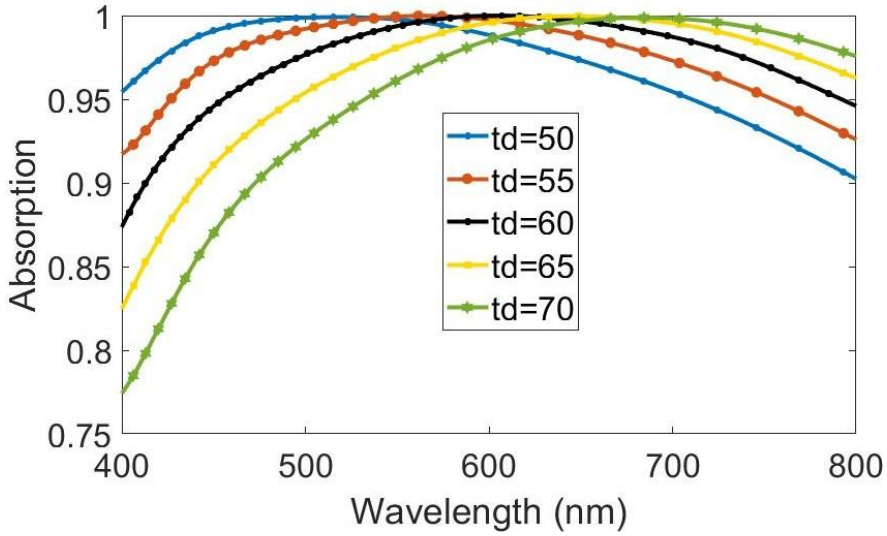

Fig. 3.4 Parametric analysis of dielectric layer thickness "td"

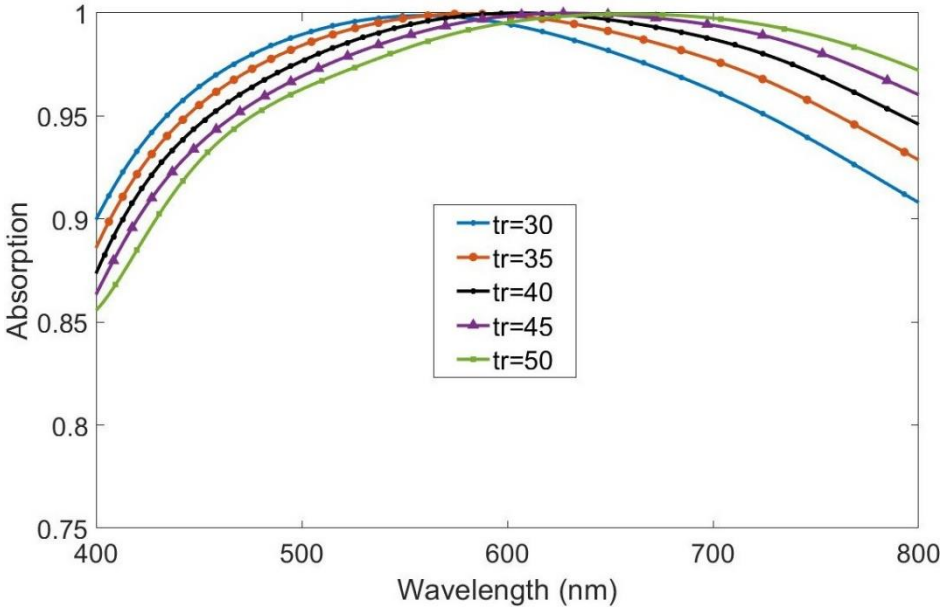

Fig. 3.5 Parametric analysis of resonator layer thickness "tr"

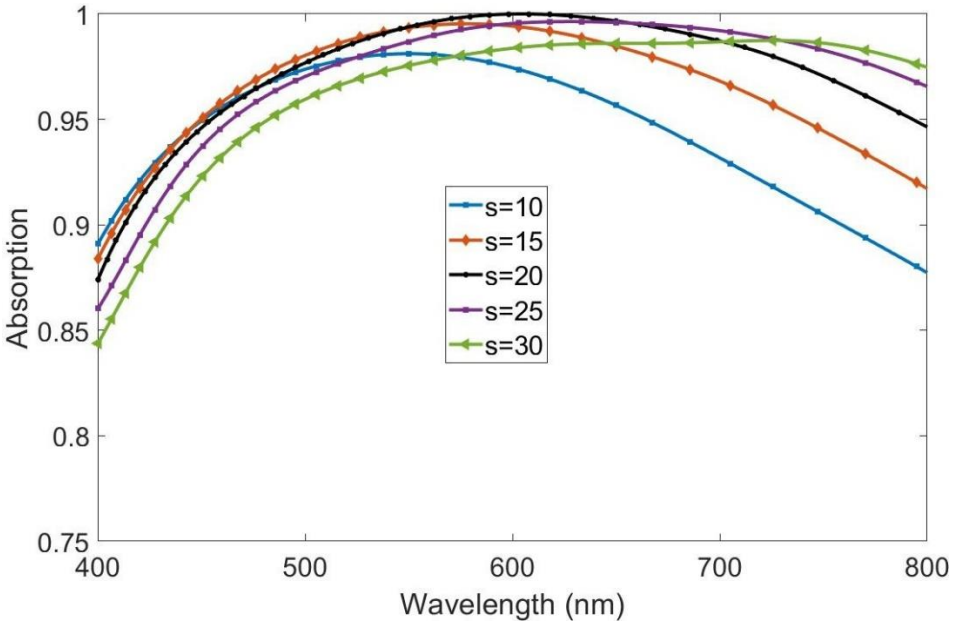

Fig. 3.6 Parametric analysis of resonator ring width "s"

3.6 Absorption comparison with different materials of dielectric layer and resonator layer

We used some dielectric and resonator materials to analyse our design. **Fig. 3.7**, and **Fig. 3.8** show how the combination of tungsten and silicon dioxide is ideal. As shown in **Fig. 3.7**, the unit cell is simulated with several metals, including silver, gold, copper, and aluminium along with tungsten. Tungsten has an excellent impedance match with a full optical region and making it ideal for the designed absorber. Only copper has a good absorption level from 450nm to 550nm, with 90% absorption. As a result, it can be employed in a variety of applications as a wideband absorber. Silver, gold, and aluminium do not absorb properly because their impedances do not meet the ideal

impedance with this design. **Fig. 3.8** is shown that the dielectric layer is replaced with four additional materials along with silicon dioxide. Indium tin oxide, gallium arsenide, Fr-4, and Silicon Amorphous are novel materials. We can see that Silicon dioxide has a significantly higher average absorption than the other materials. The varied refractive indices of certain materials are the cause of this kind of fluctuation.

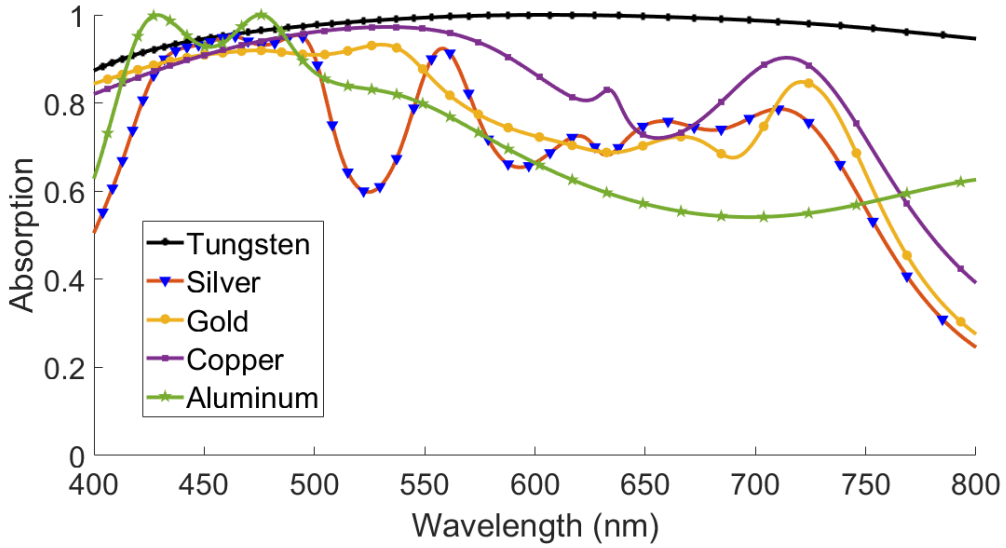

Fig. 3.7 Comparison of absorption with different materials of resonator layer

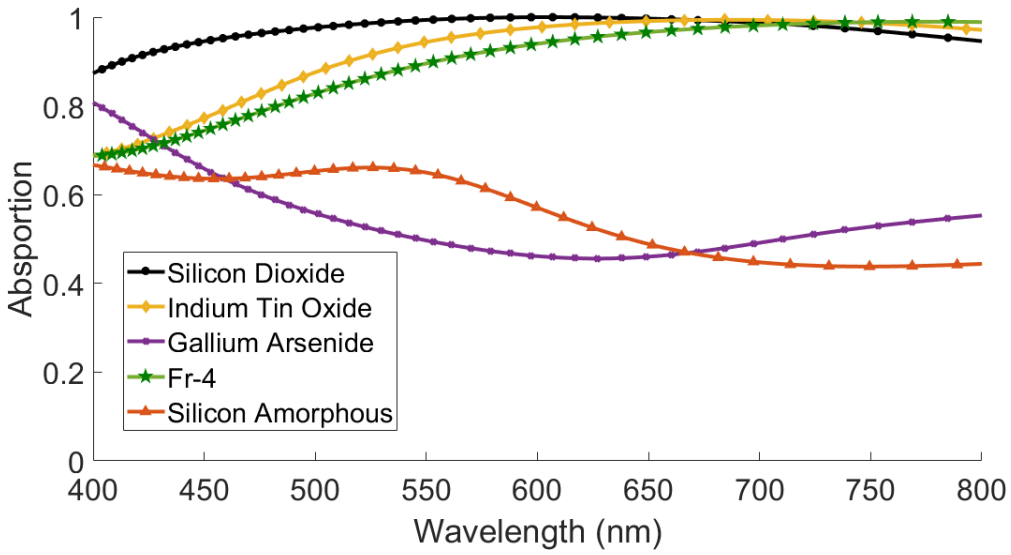

Fig. 3.8 Comparison of absorption with different materials of dielectric layer

3.7 Polarization angle insensitivity

The designed absorber absorption properties were also evaluated using a graphical depiction of the polarization angle which is shown in **Fig. 3.9** & **Fig. 9.10**. In both TE and TM mode, polarization is examined at an angle of 0° to 60°. The proposed design demonstrates excellent absorption and is almost the same in both TE and TM mode for varying polarization angles of incident EM waves ranging from 0° to 60° with a 10° increment. In TE mode, the average absorptions are 96.70%, 96.79%, 96.98%, 96.98%, 96.08%, 93.17%, and 86.63% at 0°, 10°, 20°, 30°, 40°, 50°, and 60° respectively as shown in **Fig. 3.9**. In TM mode, the average absorptions are 96.74%, 96.61%, 96.59%, 96.69%, 96.65%, 95.66%, and 92.03% at 0°, 10°, 20°, 30°, 40°, 50°, and 60° respectively as shown in **Fig. 3.10**. So, the suggested design is polarized insensitive, indicating that the applied EM wave does not affect the proposed design at certain polarization angles in the TE and TM modes. As a result of the polarization-independent features, it is realized that the design can be used to collect solar energy from sunlight in the optical regime.

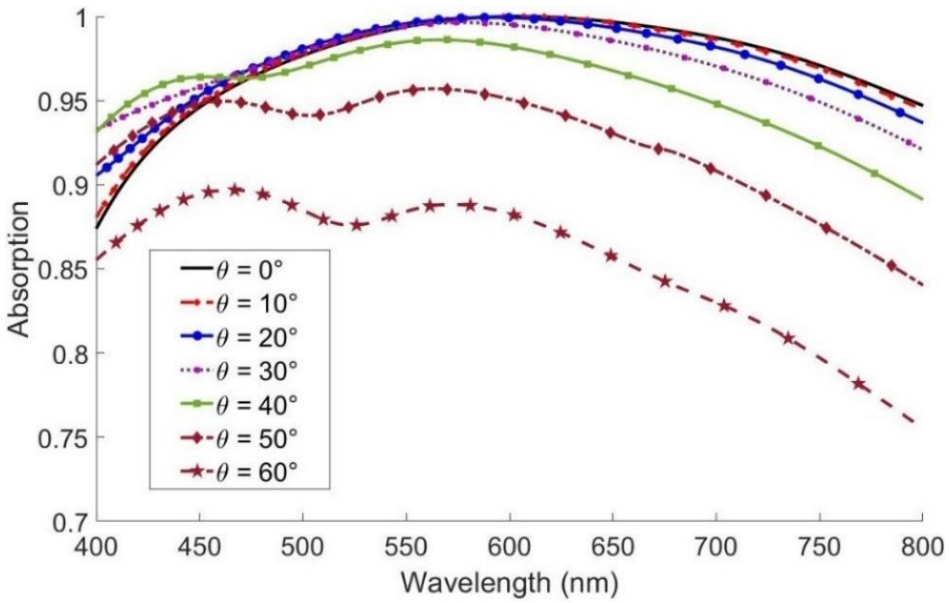

Fig. 3.9 Sensitivity of polarization angle at TE mode

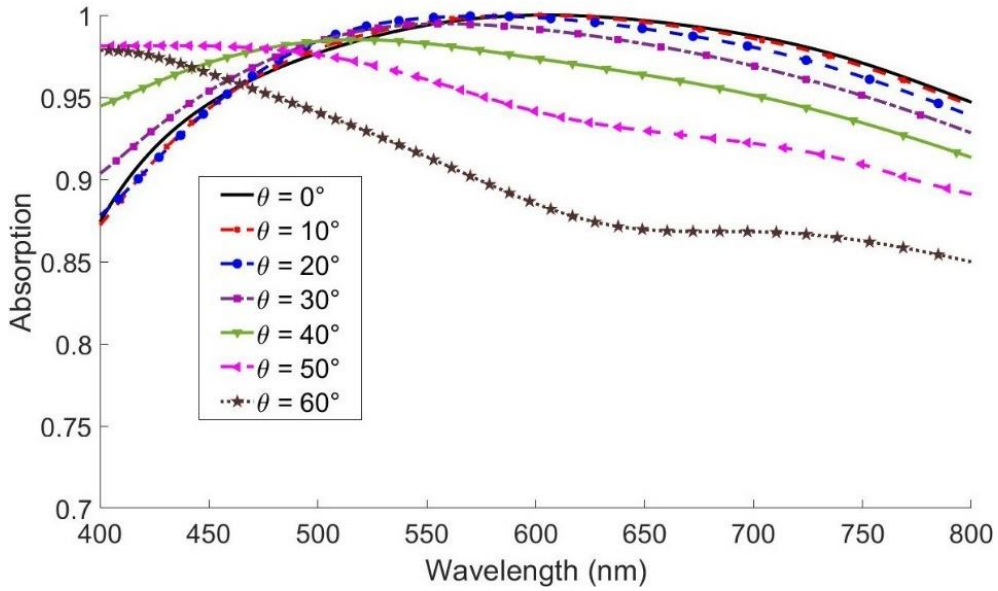

Fig. 3.10 Sensitivity of polarization angle at TM mode

3.8 Mesh view

The mesh view has something to do with performance. To improve performance and observation, the mesh view is used to divide the entire structure into several small sections. **Fig. 3.11** shows the mesh view of the designed unit cell.

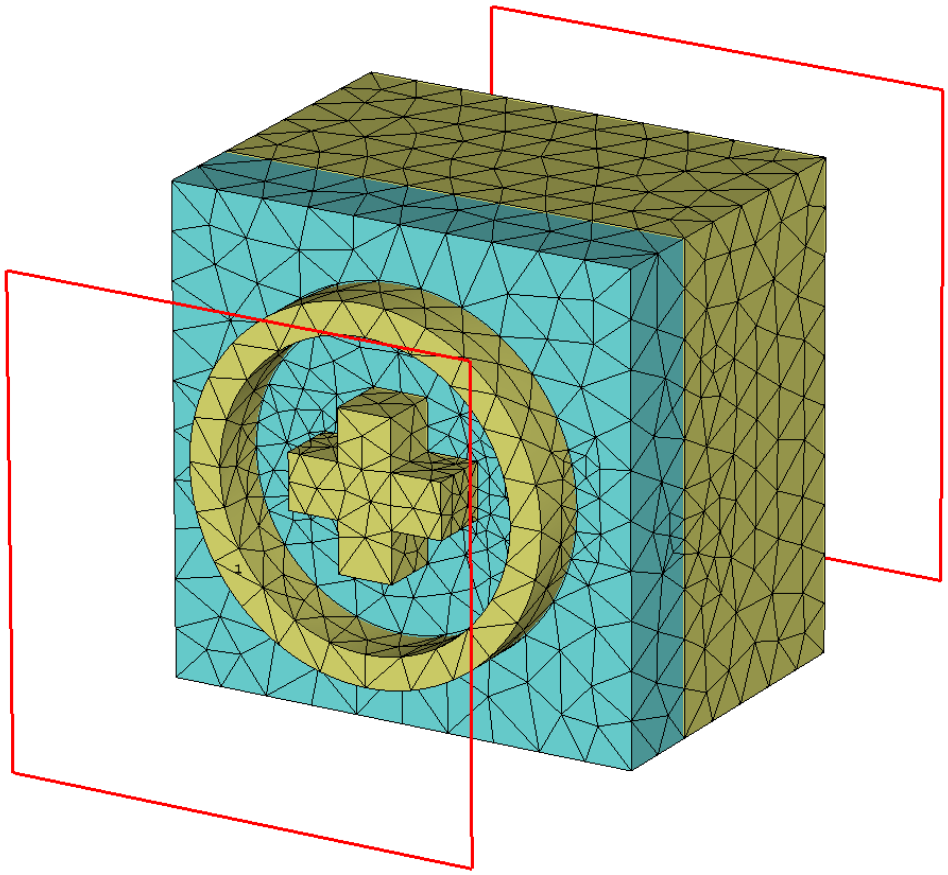

Fig. 3.11 Mesh View of the Designed unit cell

3.9 Farfield Analysis

Phi and theta parameters from field monitors presented in **Fig. 3.12** are used to analyse the waveguide, magnetic field, and electric field paths.

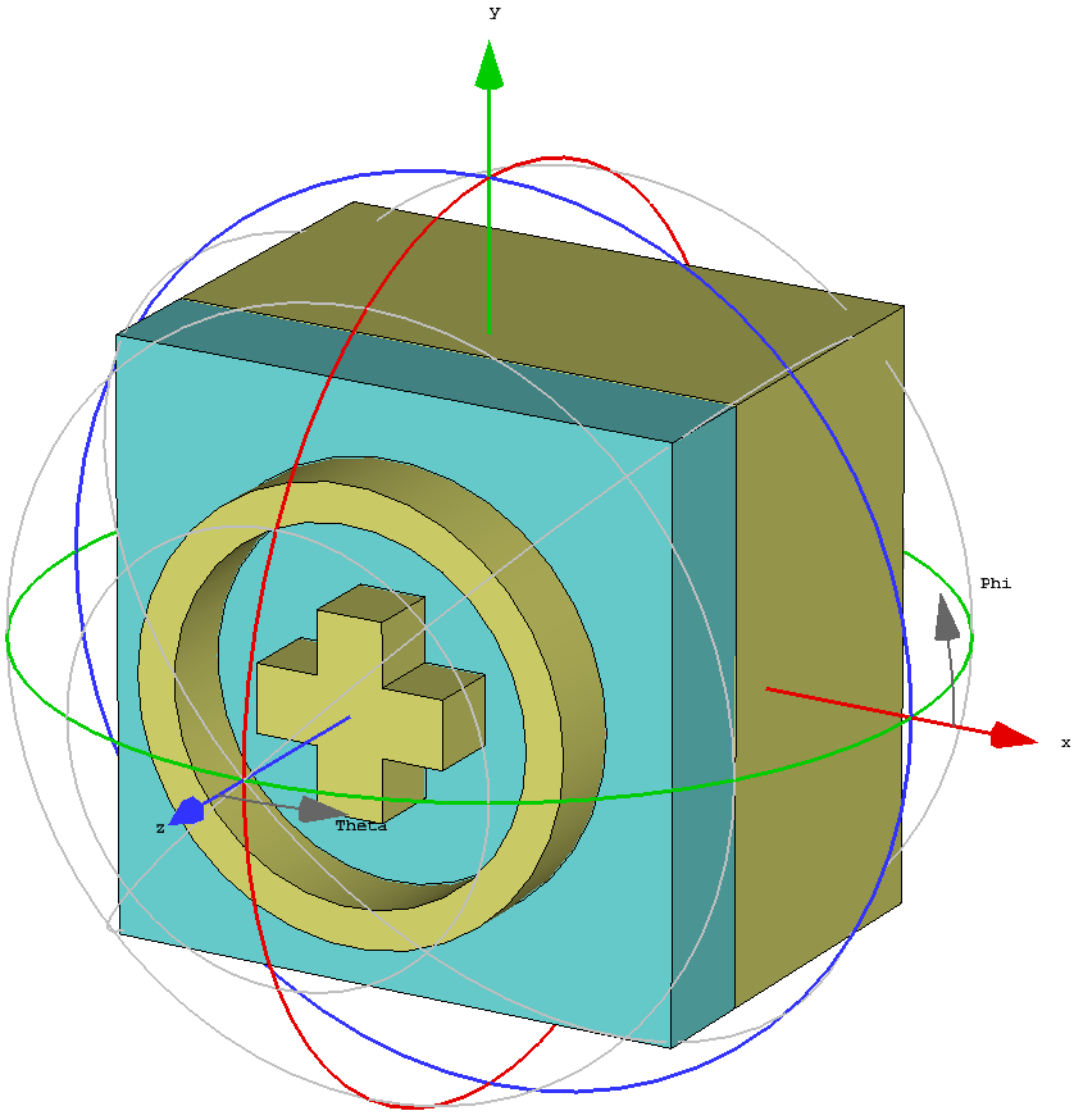

Fig. 3.12 Farfield Analysis

3.10 Analysis of E-field, H-field and surface current

The electromagnetic field and surface charge distribution are known to have a significant impact on absorption properties and energy dissipation. This section will cover the mechanism of e-field, h-field, and surface charge distribution for three wavelengths (400.15nm, 604.91nm, and 800nm). Three alternative absorption levels are used here, 87.38% (low level) at 400.15nm, 99.99%(resonance) at 604.91nm, and 94.55%(mid-level) at 800nm. The absorber, which is depicted in **Fig. 3.13 (a)-(f)** for both TE and TM mode, created a high electromagnetic field. As can be seen in **Fig. 3.13**, the dielectric

layer does an excellent job of containing the electric wave. And, as seen in **Fig. 3.14**, the magnetic wave has good confinement. As a result, surface plasmons increased and produced a very good polarization-insensitive absorber for both TE and TM modes with a good tungsten impedance match. Only the direction of propagation changed when the EM mode was altered. As previously stated, the back-layer limits transmission because the metal is chosen in a specific thickness to do so. It's also evident that the dielectric layer, not the metal layer, is primarily responsible for EM wave confinement. In the structure shown in **Fig. 3.15**, a good anti-parallel circulating current is created with good E-field and H-field. Surface charges are widely dispersed throughout the structure, particularly at the resonance wavelength, where they achieved the best results of peak 99.99% for TE and TM mode. From the above, it is obvious that the design is a good absorber for the entire optical region, with a strong electromagnetic field and surface current distribution, which will enable its application in related industries.

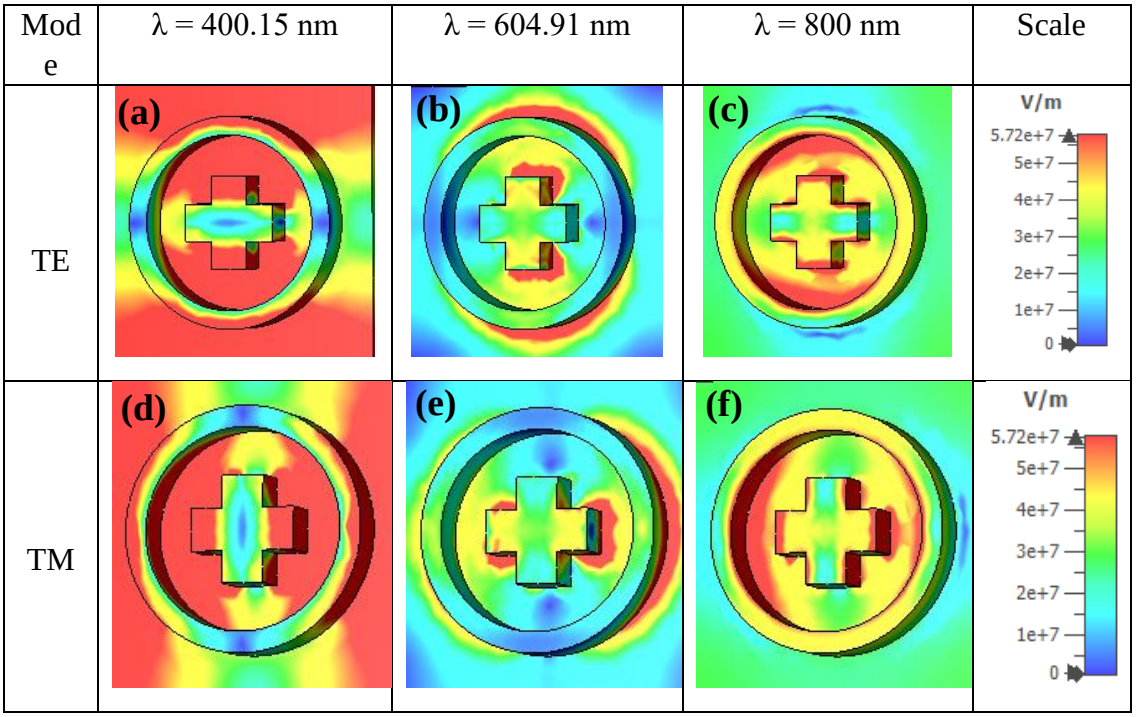

Fig. 3.13 Representation of the unit cell's electric-field distribution (a)-(c) for TE polarization in 400.15nm, 604.91nm, and 800nm using a linear colour bar (Vm^{-1}) in the y-x axis, and (d)-(f) for TM polarization in 400.15nm, 604.91nm, and 800nm using the same linear colour bar (Vm^{-1}) in the y-x axis.

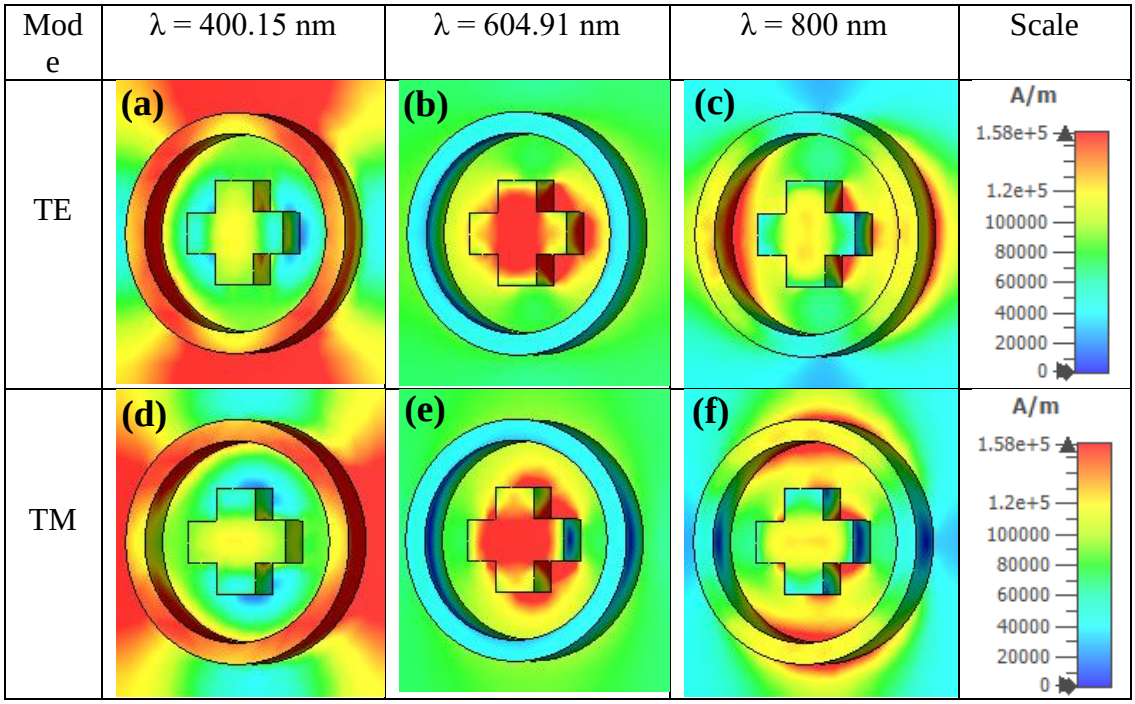

Fig. 3.14 Representation of the unit cell's magnetic-field distribution (a)-(c) for TE polarization in 400.15nm, 604.91nm, and 800nm using a linear colour bar (Am^{-1}) in the y-x axis, and (d)-(f) for TM polarization in 400.15nm, 604.91nm, and 800nm using the same linear colour bar (Am^{-1}) in the y-x axis.

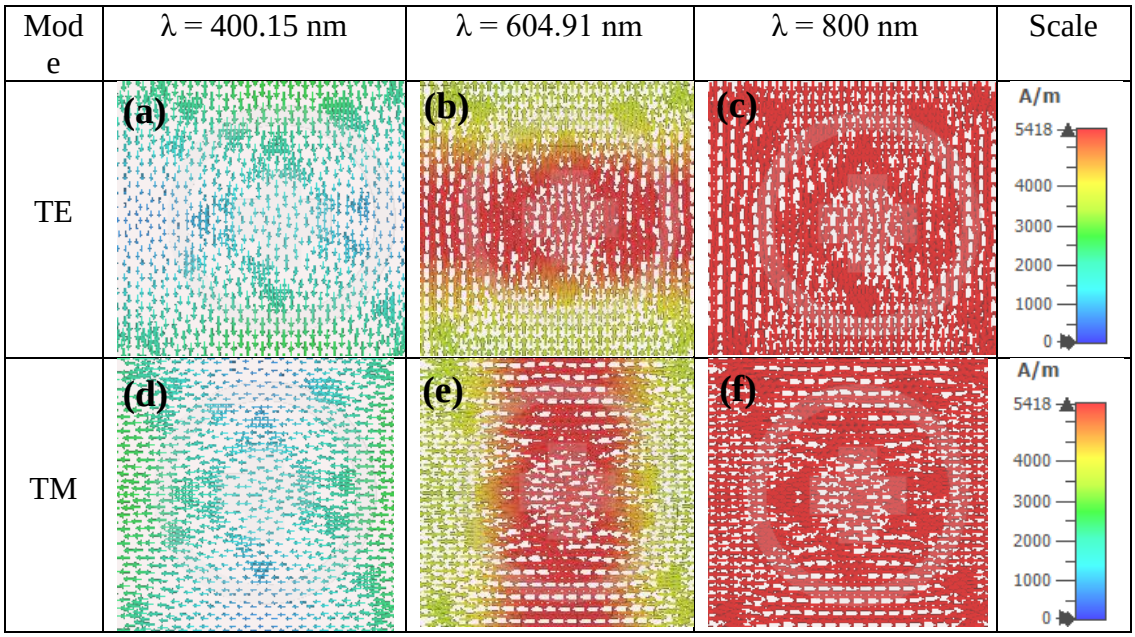

Fig. 3.15 Representation of the unit cell's surface current distribution (a)-(c) for TE mode in 400.15nm, 604.91nm, and 800nm using a linear colour bar (Am^{-1}) in the y-x axis, and (d)-(f) for TM mode in 400.15nm, 604.91nm, and 800nm using the same linear colour bar (Am^{-1}) in the y-x axis.

3.11 Comparative study

This topic explains comparative analysis based on previous work. The bandwidth, number of layers, materials utilized, polarization sensitivity and angle, absorption, and peak value are all considered here to compare with other work. This work is best considering all the comparable parameters. **Table 3.1** shows a comparison of this work with earlier work on nano-structured metamaterial absorbers. This work found an excellent absorption level when compared to earlier work with a wide-angle sensitivity, as can be seen from the table. Perfect optical wavelength absorbers that can function over a wide range of wavelengths are uncommon. Moreover, we found a perfect absorbance in optical wavelengths, with an average absorption of 96.62% and a resonance absorbance of 99.99%. The cause of high absorption is tungsten's superior impedance match. According to peak absorption level, our structure is the best design, and also our design's absorption level is higher than other similar designs in **Table 3.1**. In terms of the extreme melting point of Tungsten and SiO_2, low-materials cost, efficiency, and operational region compared with other materials used in the table below, makes this design a unique. As a result, our proposed absorber has a higher absorption performance than the other absorbers in **Table 3.1**

Table 3.1 Comparison with previous works

Ref	Bandwidth (nm)	Number of layers	Materials	Polarization sensitivity & Angle	Absorption (%)	Peak value (%)
[44]	300	Three	Ag, SiO_2	Yes, $\theta \leq 60°$	Above 90	98
[48]	308	Three	W, SiO_2	Yes, $\theta \leq 60°$	Above 91.24	99.99
[65]	140.4	Three	Au, SiO_2, Si	Yes, $\theta \leq 80°$	Above 80	98.2
[69]	300	Four	Cu, Si_3N_4, Si	No, N/A	Above 80	97
[100]	300	Three	Ni, Si	Yes, $\theta \leq 60°$	Above 90	99
[101]	380	Three	Au, SiO_2	No, N/A	Above 83	92
[102]	400	Two	Au, Si	Yes, $\theta \leq 50°$	Above 90	99.1
[103]	310	Multi	Au, Si	Yes, $\theta \leq 65°$	Above 80	98.5
[104]	300	Three	Ag, SiO_2	No, N/A	Above 80	98
[105]	350	Three	Au, SiO_2, Al	Yes, $\theta \leq 60°$	Above 80	99
[106]	350	Four	SiO_2-Au	Yes, $\theta \leq 60°$	Above 85	99
[107]	300	Multi	Au, Si	Yes, $\theta \leq 60°$	Above 91	99.95
[108]	311	Three	W, SO_2	Yes, $\theta \leq 30°$	Above 85	99
[109]	375	Three	W, Quartz	Yes, $\theta \leq 45°$	Above 66.66	99.92
[110]	380	Three	A-Si, Ag, ITO	Yes, $\theta \leq 50°$	Above 90	99
This work	300	Three	W, SiO_2	Yes, $\theta \leq 60°$	Above 94.5	99.99

CHAPTER 4
CONCLUSIONS AND FUTURE WORK

4.1 Introduction

Our goal was to create a perfect material absorber that could absorb more than 96% of absorption. Our objective was met. More than 96.5% absorption was achieved in this work. These have already been covered in previous chapters. In this chapter, the summary of this work and the future work are discussed.

4.2 Conclusions

This work developed a polarization-insensitive, broadband, wide-angle metamaterial absorber for optical wavelengths ranging from 400 to 800 nm. The traditional three-layer approach with a metal-dielectric-metal structure was used. The structure has a wide bandwidth and practically perfect absorbance above 94.58% at all locations, with 99.99% peak points. With an average absorption of 96.62%, it also displayed polarization angle independent behaviour. Better absorption was accomplished with the structure due to a good impedance match of tungsten and the lossless features of silicon dioxide (SiO_2). Because its resonance alters with changes in its dielectric layer and resonator thickness, this metamaterial absorber could be used as an optical sensor. It could be used in solar energy collecting applications or as a solar sensor because of its angular independence. This absorber is also ideal for solar thermophotovoltaic, and solar cell applications due to the high melting point of tungsten and silicon dioxide and the wide incident angle.

4.3 Future work

Perfect Metamaterial Absorbers are a promising candidate among several types of absorbing components. Metamaterial absorbers, particularly in solar harvesting, can provide a significant gain in inefficiency. In the future, these absorbers could be used in a variety of commercial and military applications, including transparent and flexible materials. Such a metamaterial absorber can be used to create Tetra Hertz thermal imaging technology. For such applications, they have a low volume and density, as well as a narrow band response.

REFERENCES

[1] P. V. Kamat, “Meeting the clean energy demand: Nanostructure architectures for solar energy conversion,” *J. Phys. Chem. C*, vol. 111, no. 7, pp. 2834–2860, 2007, doi: 10.1021/jp066952u.

[2] C. G. Granqvist, “Solar Energy Materials,” *Adv. Mater.*, vol. 15, no. 21, pp. 1789–1803, 2003, doi: 10.1002/adma.200300378.

[3] S. R. Bull, “Renewable energy today and tomorrow,” *Proc. IEEE*, vol. 89, no. 8, pp. 1216–1226, 2001, doi: 10.1109/5.940290.

[4] H. Lund, “Renewable energy strategies for sustainable development,” *Energy*, vol. 32, no. 6, pp. 912–919, 2007, doi: 10.1016/j.energy.2006.10.017.

[5] R. S. Kshetrimayum, “A brief intro to metamaterials,” *IEEE Potentials*, vol. 23, no. 5, pp. 44–46, 2004, doi: 10.1109/MP.2005.1368916.

[6] N. I. Landy, S. Sajuyigbe, J. J. Mock, D. R. Smith, and W. J. Padilla, “Perfect metamaterial absorber,” *Phys. Rev. Lett.*, vol. 100, no. 20, 2008, doi: 10.1103/PhysRevLett.100.207402.

[7] V. G. Veselago, “The Electrodynamic of Substances with Simultaneous Negative Values of e and μ,” *Sov. Phys. Uspekhi*, vol. 10, no. 4, pp. 509–514, 1968.

[8] D. R. Smith, J. B. Pendry, and M. C. K. Wiltshire, “Metamaterials and negative refractive index,” *Science (80-.).*, vol. 305, no. 5685, pp. 788–792, 2004, doi: 10.1126/science.1096796.

[9] K. Gangwar, Paras, and R. P. S. Gangwar, “Metamaterials: Characteristics, Process and Applications,” *Adv. Electron. Electr. Eng.*, vol. 4, no. 1, pp. 97–106, 2014, [Online]. Available: http://www.ripublication.com/aeee_spl/aeeev4n1spl_14.pdf.

[10] M. M. Hasan, M. R. I. Faruque, and M. T. Islam, “Dual band metamaterial antenna for LTE/bluetooth/WiMAX system,” *Sci. Rep.*, vol. 8, no. 1, pp. 1–17, 2018, doi: 10.1038/s41598-018-19705-3.

[11] T. Alam, M. R. I. Faruque, and M. T. Islam, “A double-negative metamaterial-inspired mobile wireless antenna for electromagnetic absorption reduction,” *Materials (Basel).*, vol. 8, no. 8, pp. 4817–4828, 2015, doi: 10.3390/ma8084817.

[12] M. Alibakhshikenari *et al.*, “Study on on-Chip Antenna Design Based on Metamaterial-Inspired and Substrate-Integrated Waveguide Properties for Millimetre-Wave and THz Integrated-Circuit Applications,” *J. Infrared, Millimeter, Terahertz Waves*, vol. 42, no. 1, pp. 17–28, 2021, doi: 10.1007/s10762-020-00753-8.

[13] M. Chen, H. Jiang, H. Zhang, D. Li, and Y. Wang, “Design of an acoustic superlens using single-phase metamaterials with a star-shaped lattice structure,” *Sci. Rep.*, vol. 8, no. 1, pp. 2–9, 2018, doi: 10.1038/s41598-018-19374-2.

[14] X. Zhang and Z. Liu, “Superlenses to overcome the diffraction limit,” *Nat. Mater.*, vol. 7, no. 6, pp. 435–441, 2008, doi: 10.1038/nmat2141.

[15] D. Schurig, “An aberration-free lens with zero F-number,” *New J. Phys.*, vol. 10, 2008, doi: 10.1088/1367-2630/10/11/115034.

[16] G. Yuan, K. S. Rogers, E. T. F. Rogers, and N. I. Zheludev, “Far-Field Superoscillatory Metamaterial Superlens,” *Phys. Rev. Appl.*, vol. 11, no. 6, p. 1, 2019, doi: 10.1103/PhysRevApplied.11.064016.

[17] M. M. K. Shuvo, M. I. Hossain, S. Rahman, S. Mahmud, S. S. Islam, and M. T. Islam, "A Wide-Angle, Enhanced Oblique Incidence, Bend-Able Metamaterial Absorber Employed in Visible Region with a Sun Shape Resonator," *IEEE Access*, vol. 9, pp. 126466–126480, 2021, doi: 10.1109/ACCESS.2021.3111813.

[18] N. Engheta, "An idea for thin subwavelength cavity resonators using metamaterials with negative permittivity and permeability," *IEEE Antennas Wirel. Propag. Lett.*, vol. 1, pp. 10–13, 2002, doi: 10.1109/LAWP.2002.802576.

[19] S. Molesky and Z. Jacob, "High temperature Epsilon-near-Zero and Epsilon-near-Pole metamaterial emitters for thermophotovoltaics," *2013 Conf. Lasers Electro-Optics, CLEO 2013*, vol. 21, no. January, pp. 549–554, 2013, doi: 10.1364/cleo_qels.2013.qtu1a.6.

[20] M. Gil, J. Bonache, J. García-García, J. Martel, and F. Martín, "Composite right/left-handed metamaterial transmission lines based on complementary split-rings resonators and their applications to very wideband and compact filter design," *IEEE Trans. Microw. Theory Tech.*, vol. 55, no. 6, pp. 1296–1303, 2007, doi: 10.1109/TMTT.2007.897755.

[21] H. Zhu and F. Semperlotti, "Metamaterial based embedded acoustic filters for structural applications," *AIP Adv.*, vol. 3, no. 9, 2013, doi: 10.1063/1.4822157.

[22] S. S. Islam, M. R. I. Faruque, and M. T. Islam, "A near zero refractive index metamaterial for electromagnetic invisibility cloaking operation," *Materials (Basel).*, vol. 8, no. 8, pp. 4790–4804, 2015, doi: 10.3390/ma8084790.

[23] N. Landy and D. R. Smith, "A full-parameter unidirectional metamaterial cloak for microwaves," *Nat. Mater.*, vol. 12, no. 1, pp. 25–28, 2013, doi: 10.1038/nmat3476.

[24] D. Schurig *et al.*, "Metamaterial electromagnetic cloak at microwave frequencies," *Science (80-.).*, vol. 314, no. 5801, pp. 977–980, 2006, doi: 10.1126/science.1133628.

[25] G. Duan, X. Zhao, S. W. Anderson, and X. Zhang, "Boosting magnetic resonance imaging signal-to-noise ratio using magnetic metamaterials," *Commun. Phys.*, vol. 2, no. 1, pp. 1–8, 2019, doi: 10.1038/s42005-019-0135-7.

[26] X. Zhao, G. Duan, K. Wu, S. W. Anderson, and X. Zhang, "Intelligent Metamaterials Based on Nonlinearity for Magnetic Resonance Imaging," *Adv. Mater.*, vol. 31, no. 49, pp. 1–7, 2019, doi: 10.1002/adma.201905461.

[27] J. Y. Suen *et al.*, "Multifunctional metamaterial pyroelectric infrared detectors," *Optica*, vol. 4, no. 2, p. 276, 2017, doi: 10.1364/optica.4.000276.

[28] X. Yin *et al.*, "Ultra-wideband microwave absorber by connecting multiple absorption bands of two different-sized hyperbolic metamaterial waveguide arrays," *Sci. Rep.*, vol. 5, no. September, pp. 1–8, 2015, doi: 10.1038/srep15367.

[29] J. Luo, P. Xu, H. Chen, B. Hou, L. Gao, and Y. Lai, "Realizing almost perfect bending waveguides with anisotropic epsilon-near-zero metamaterials," *Appl. Phys. Lett.*, vol. 100, no. 22, pp. 2010–2015, 2012, doi: 10.1063/1.4723844.

[30] A. Tyszka-Zawadzka, B. Janaszek, and P. Szczepański, "Tunable slow light in graphene-based hyperbolic metamaterial waveguide operating in SCLU telecom bands," *Opt. Express*, vol. 25, no. 7, p. 7263, 2017, doi: 10.1364/oe.25.007263.

[31] F. Fan *et al.*, “Terahertz transmission and sensing properties of microstructured PMMA tube waveguide,” *Opt. Express*, vol. 23, no. 21, p. 27204, 2015, doi: 10.1364/oe.23.027204.

[32] D. Sim, J. H. Kwon, and Y. J. Yoon, “in Wearable Applications,” pp. 1–4, 2016.

[33] F. Hu *et al.*, “Design of a polarization insensitive multiband terahertz metamaterial absorber,” *J. Phys. D. Appl. Phys.*, vol. 46, no. 19, 2013, doi: 10.1088/0022-3727/46/19/195103.

[34] T. Han *et al.*, “Manipulating Steady Heat Conduction by Sensu-shaped Thermal Metamaterials,” *Sci. Rep.*, vol. 5, pp. 1–7, 2015, doi: 10.1038/srep10242.

[35] M. A. Kats and F. Capasso, “Optical absorbers based on strong interference in ultra-thin films,” *Laser Photonics Rev.*, vol. 10, no. 5, pp. 735–749, 2016, doi: 10.1002/lpor.201600098.

[36] A. Hoque and M. T. Islam, “Numerical Analysis of Single Negative Broadband Metamaterial Absorber Based on Tri Thin Layer Material in Visible Spectrum for Solar Cell Energy Harvesting,” *Plasmonics*, vol. 15, no. 4, pp. 1061–1069, 2020, doi: 10.1007/s11468-020-01132-8.

[37] H. Zhai, C. Zhan, Z. Li, and C. Liang, “A triple-band ultrathin metamaterial absorber with wide-angle and polarization stability,” *IEEE Antennas Wirel. Propag. Lett.*, vol. 14, pp. 241–244, 2015, doi: 10.1109/LAWP.2014.2361011.

[38] L. Xie, W. Gao, J. Shu, Y. Ying, and J. Kono, “Extraordinary sensitivity enhancement by metasurfaces in terahertz detection of antibiotics,” *Sci. Rep.*, vol. 5, pp. 1–4, 2015, doi: 10.1038/srep08671.

[39] H. K. Kim, D. Lee, and S. Lim, “A fluidically tunable metasurface absorber for flexible large-scale wireless ethanol sensor applications,” *Sensors (Switzerland)*, vol. 16, no. 8, 2016, doi: 10.3390/s16081246.

[40] Y. Cheng, F. Chen, and H. Luo, “Triple-Band Perfect Light Absorber Based on Hybrid Metasurface for Sensing Application,” *Nanoscale Res. Lett.*, vol. 15, no. 1, 2020, doi: 10.1186/s11671-020-03332-x.

[41] S. Mahmud, S. S. Islam, A. F. Almutairi, and M. T. Islam, “A Wide Incident Angle, Ultrathin, Polarization-Insensitive Metamaterial Absorber for Optical Wavelength Applications,” *IEEE Access*, vol. 8, no. July, pp. 129525–129541, 2020, doi: 10.1109/ACCESS.2020.3008429.

[42] Q. Li *et al.*, “Tunable perfect narrow-band absorber based on a metal-dielectric-metal structure,” *Coatings*, vol. 9, no. 6, pp. 1–11, 2019, doi: 10.3390/COATINGS9060393.

[43] K. Aydin, V. E. Ferry, R. M. Briggs, and H. A. Atwater, “Broadband polarization-independent resonant light absorption using ultrathin plasmonic super absorbers,” *Nat. Commun.*, vol. 2, no. 1, p. 517, 2011, doi: 10.1038/ncomms1528.

[44] X. Zhang, Y. Fan, L. Qi, and H. Li, “Broadband plasmonic metamaterial absorber with fish-scale structure at visible frequencies,” *Opt. Mater. Express*, vol. 6, no. 7, p. 2448, 2016, doi: 10.1364/ome.6.002448.

[45] Y. Qiu Xu, P. Heng Zhou, H. Bin Zhang, L. Chen, and L. Jiang Deng, “A wide-angle planar metamaterial absorber based on split ring resonator coupling,” *J. Appl. Phys.*, vol. 110, no. 4, 2011, doi: 10.1063/1.3622675.

[46] Y. Liu, Y. Chen, J. Li, T. chen Hung, and J. Li, “Study of energy absorption on solar cell using

metamaterials," *Sol. Energy*, vol. 86, no. 5, pp. 1586–1599, 2012, doi: 10.1016/j.solener.2012.02.021.

[47] S. Lee, T. Q. Tran, H. Heo, M. Kim, and S. Kim, "A proposal of a perfect graphene absorber with enhanced design and fabrication tolerance," *Sci. Rep.*, vol. 7, no. 1, pp. 1–10, 2017, doi: 10.1038/s41598-017-04995-w.

[48] S. Mahmud, S. S. Islam, K. Mat, M. E. H. Chowdhury, H. Rmili, and M. T. Islam, "Design and parametric analysis of a wide-angle polarization-insensitive metamaterial absorber with a star shape resonator for optical wavelength applications," *Results Phys.*, vol. 18, no. July, p. 103259, 2020, doi: 10.1016/j.rinp.2020.103259.

[49] N. Mattiucci, M. J. Bloemer, N. Aközbek, and G. D'aguanno, "Impedance matched thin metamaterials make metals absorbing," *Sci. Rep.*, vol. 3, pp. 1–11, 2013, doi: 10.1038/srep03203.

[50] K. A. Willets and R. P. Van Duyne, "Localized surface plasmon resonance spectroscopy and sensing," *Annu. Rev. Phys. Chem.*, vol. 58, pp. 267–297, 2007, doi: 10.1146/annurev.physchem.58.032806.104607.

[51] H. Tong, Y. Xu, Y. Su, and X. Wang, "Theoretical study for fabricating elliptical subwavelength nanohole arrays by higher-order waveguide-mode interference," *Results Phys.*, vol. 14, no. June, p. 102460, 2019, doi: 10.1016/j.rinp.2019.102460.

[52] S. Liu *et al.*, "A bi-layered quad-band metamaterial absorber at terahertz frequencies," *J. Appl. Phys.*, vol. 118, no. 24, 2015, doi: 10.1063/1.4938110.

[53] M. H. Li, H. L. Yang, X. W. Hou, Y. Tian, and D. Y. Hou, "Perfect metamaterial absorber with dual bands," *Prog. Electromagn. Res.*, vol. 108, no. July, pp. 37–49, 2010, doi: 10.2528/PIER10071409.

[54] C. M. Tran, H. Van Pham, H. T. Nguyen, T. T. Nguyen, L. D. Vu, and T. H. Do, "Creating Multiband and Broadband Metamaterial Absorber by Multiporous Square Layer Structure," *Plasmonics*, vol. 14, no. 6, pp. 1587–1592, 2019, doi: 10.1007/s11468-019-00953-6.

[55] J. Fan, D. Xiao, Q. Wang, Q. Liu, and Z. Ouyang, "Wide-angle broadband terahertz metamaterial absorber with a multilayered heterostructure," *Appl. Opt.*, vol. 56, no. 15, p. 4388, 2017, doi: 10.1364/ao.56.004388.

[56] P. Fu, F. Liu, G. J. Ren, F. Su, D. Li, and J. Q. Yao, "A broadband metamaterial absorber based on multi-layer graphene in the terahertz region," *Opt. Commun.*, vol. 417, no. November 2017, pp. 62–66, 2018, doi: 10.1016/j.optcom.2018.02.034.

[57] D. verma Atul, "d M us pt," *Certain distance degree based Topol. indices Zeolite LTA Fram.*, no. December 2016, pp. 11–14, 2018.

[58] H. Xiong, J. S. Hong, C. M. Luo, and L. L. Zhong, "An ultrathin and broadband metamaterial absorber using multi-layer structures," *J. Appl. Phys.*, vol. 114, no. 6, 2013, doi: 10.1063/1.4818318.

[59] M. Zhong, "Enhance of the absorption and bandwidth based on a ultra-thin tungsten structure metamaterial absorber in 400–1500 nm range," *Opt. Laser Technol.*, vol. 127, no. December 2019, p. 106142, 2020, doi: 10.1016/j.optlastec.2020.106142.

[60] H. Cao, M. Shan, T. Chen, J. Lei, L. Yang, and X. Tan, “Triple-band polarization-independent ultrathin metamaterial absorber,” *Prog. Electromagn. Res. M*, vol. 77, no. November 2018, pp. 93–102, 2019, doi: 10.2528/pierm18110602.

[61] K. P. Kaur, T. Upadhyaya, M. Palandoken, and C. Gocen, “Ultrathin dual-layer triple-band flexible microwave metamaterial absorber for energy harvesting applications,” *Int. J. RF Microw. Comput. Eng.*, vol. 29, no. 1, pp. 1–7, 2019, doi: 10.1002/mmce.21646.

[62] A. Sarkhel and S. R. B. Chaudhuri, “Compact quad-band polarization-insensitive ultrathin metamaterial absorber with wide angle stability,” *IEEE Antennas Wirel. Propag. Lett.*, vol. 16, no. c, pp. 3240–3244, 2017, doi: 10.1109/LAWP.2017.2768077.

[63] B. Zhu, Z. Wang, C. Huang, Y. Feng, J. Zhao, and T. Jiang, “Polarization insensitive metamaterial absorber with wide incident angle,” *Prog. Electromagn. Res.*, vol. 101, pp. 231–239, 2010, doi: 10.2528/PIER10011110.

[64] F. Qin *et al.*, “Ultra-broadband and wide-angle perfect solar absorber based on TiN nanodisk and Ti thin film structure,” *Sol. Energy Mater. Sol. Cells*, vol. 211, no. March, p. 110535, 2020, doi: 10.1016/j.solmat.2020.110535.

[65] W. Zhu *et al.*, “Wideband visible-light absorption in an ultrathin silicon nanostructure,” *Opt. Express*, vol. 25, no. 5, p. 5781, 2017, doi: 10.1364/oe.25.005781.

[66] I. Hossain, A. F. Almutairi, A. Hoque, and M. Tariqul, “Hexagonal Resonator Loaded Star Shaped Polarization Insensitive Compact Broadband Zero Indexed Nano-Meta Absorber for Optical Region Applications: A Numerical Approach,” *Res. Sq.*, [Online]. Available: https://www.researchsquare.com/article/rs-151084/latest?utm_source=researcher_app&utm_medium=referral&utm_campaign=RESR_MRKT_Researcher_inbound.

[67] P. Rufangura and C. Sabah, “Dual-band perfect metamaterial absorber for solar cell applications,” *Vacuum*, vol. 120, pp. 68–74, 2015, doi: 10.1016/j.vacuum.2015.05.033.

[68] M. H. Heidari and S. H. Sedighy, “Broadband wide-angle polarization-insensitive metasurface solar absorber,” *J. Opt. Soc. Am. A*, vol. 35, no. 4, p. 522, 2018, doi: 10.1364/josaa.35.000522.

[69] P. Zhu and L. Jay Guo, “High performance broadband absorber in the visible band by engineered dispersion and geometry of a metal-dielectric-metal stack,” *Appl. Phys. Lett.*, vol. 101, no. 24, 2012, doi: 10.1063/1.4771994.

[70] T. S. Tuan and N. T. Q. Hoa, “Numerical Study of an Efficient Broadband Metamaterial Absorber in Visible Light Region,” *IEEE Photonics J.*, vol. 11, no. 3, pp. 1–10, 2019, doi: 10.1109/JPHOT.2019.2910806.

[71] M. A. Baqir, M. Ghasemi, P. K. Choudhury, and B. Y. Majlis, “Design and analysis of nanostructured subwavelength metamaterial absorber operating in the UV and visible spectral range,” *J. Electromagn. Waves Appl.*, vol. 29, no. 18, pp. 2408–2419, 2015, doi: 10.1080/09205071.2015.1073124.

[72] P. T. Dang *et al.*, “Efficient broadband truncated-pyramid-based metamaterial absorber in the visible and near-infrared regions,” *Crystals*, vol. 10, no. 9, pp. 1–12, 2020, doi: 10.3390/cryst10090784.

[73] N. T. Q. Hoa, P. H. Lam, P. D. Tung, T. S. Tuan, and H. Nguyen, "Numerical Study of a Wide-Angle and Polarization-Insensitive Ultrabroadband Metamaterial Absorber in Visible and Near-Infrared Region," *IEEE Photonics J.*, vol. 11, no. 1, p. 1, 2019, doi: 10.1109/JPHOT.2018.2888971.

[74] L. Zigoneanu, B. I. Popa, A. F. Starr, and S. A. Cummer, "Design and measurements of a broadband two-dimensional acoustic metamaterial with anisotropic effective mass density," *J. Appl. Phys.*, vol. 109, no. 5, 2011, doi: 10.1063/1.3552990.

[75] W. Zuo, Y. Yang, X. He, D. Zhan, and Q. Zhang, "A miniaturized metamaterial absorber for ultrahigh-frequency RFID system," *IEEE Antennas Wirel. Propag. Lett.*, vol. 16, no. c, pp. 329–332, 2017, doi: 10.1109/LAWP.2016.2574885.

[76] F. Sakran, Y. Neve-Oz, A. Ron, M. Golosovsky, D. Davidov, and A. Frenkel, "Absorbing frequency-selective-surface for the mm-wave range," *IEEE Trans. Antennas Propag.*, vol. 56, no. 8 II, pp. 2649–2655, 2008, doi: 10.1109/TAP.2008.924701.

[77] N. Mishra, D. K. Choudhary, R. Chowdhury, K. Kumari, and R. K. Chaudhary, "An Investigation on Compact Ultra-Thin Triple Band Polarization Independent Metamaterial Absorber for Microwave Frequency Applications," *IEEE Access*, vol. 5, no. c, pp. 4370–4376, 2017, doi: 10.1109/ACCESS.2017.2675439.

[78] K. Shi, G. Jin, R. Liu, T. Ye, and Y. Xue, "Underwater sound absorption performance of acoustic metamaterials with multilayered locally resonant scatterers," *Results Phys.*, vol. 12, no. October 2018, pp. 132–142, 2019, doi: 10.1016/j.rinp.2018.11.060.

[79] Y. Huang, L. Liu, M. Pu, X. Li, X. Ma, and X. Luo, "A refractory metamaterial absorber for ultra-broadband, omnidirectional and polarization-independent absorption in the UV-NIR spectrum," *Nanoscale*, vol. 10, no. 17, pp. 8298–8303, 2018, doi: 10.1039/c8nr01728j.

[80] P. V. Tuong, J. W. Park, V. D. Lam, W. H. Jang, S. A. Nikitov, and Y. P. Lee, "Dielectric and Ohmic losses in perfectly absorbingmetamaterials," *Opt. Commun.*, vol. 295, pp. 17–20, 2013, doi: 10.1016/j.optcom.2013.01.031.

[81] M. A. Baqir and P. K. Choudhury, "Hyperbolic Metamaterial-Based UV Absorber," *IEEE Photonics Technol. Lett.*, vol. 29, no. 18, pp. 1548–1551, 2017, doi: 10.1109/LPT.2017.2735453.

[82] S. Mahmud *et al.*, "A Multi-Band Near Perfect Polarization and Angular Insensitive Metamaterial Absorber With a Simple Octagonal Resonator for Visible Wavelength," *IEEE Access*, vol. 9, pp. 117746–117760, 2021, doi: 10.1109/access.2021.3106588.

[83] A. Xomalis *et al.*, "Cryptography in coherent optical information networks using dissipative metamaterial gates," *APL Photonics*, vol. 4, no. 4, 2019, doi: 10.1063/1.5092216.

[84] C. Liang *et al.*, "A broadband and polarization-independent metamaterial perfect absorber with monolayer Cr and Ti elliptical disks array," *Results Phys.*, vol. 15, no. September, p. 102635, 2019, doi: 10.1016/j.rinp.2019.102635.

[85] P. Moitra *et al.*, "Large-Scale All-Dielectric Metamaterial Perfect Reflectors," *ACS Photonics*, vol. 2, no. 6, pp. 692–698, 2015, doi: 10.1021/acsphotonics.5b00148.

[86] Y. Tang *et al.*, "Hybrid acoustic metamaterial as super absorber for broadband low-frequency sound," *Sci. Rep.*, vol. 7, no. July 2016, pp. 1–10, 2017, doi: 10.1038/srep43340.

[87] X. Wang, “Uncooled CMOS Integrated Triple-Band Terahertz Thermal Detector Comprising of Metamaterial Absorber and PTAT Sensor,” *IEEE Access*, vol. 8, pp. 114501–114508, 2020, doi: 10.1109/ACCESS.2020.3004344.

[88] Y. Gong *et al.*, “Highly flexible all-optical metamaterial absorption switching assisted by Kerr-nonlinear effect,” *Opt. Express*, vol. 19, no. 11, p. 10193, 2011, doi: 10.1364/oe.19.010193.

[89] S. Perhirin and Y. Auffret, “A low consumption electronic system developed for a 10km long all-optical extension dedicated to sea floor observatories using power-over-fiber technology and SPI protocol.,” *Microw. Opt. Technol. Lett.*, vol. 55, no. 11, pp. 2562–2568, 2013, doi: 10.1002/mop.

[90] A. Ennajih, J. Zbitou, M. Latrach, A. Errkik, and R. Mandry, “A new dual band printed metamaterial antenna for RFID reader applications,” *Int. J. Electr. Comput. Eng.*, vol. 7, no. 6, pp. 3507–3514, 2017, doi: 10.11591/ijece.v7i6.pp3507-3514.

[91] A. S. Dhillon, D. Mittal, and R. Bargota, “Triple band ultrathin polarization insensitive metamaterial absorber for defense, explosive detection and airborne radar applications,” *Microw. Opt. Technol. Lett.*, vol. 61, no. 1, pp. 89–95, 2019, doi: 10.1002/mop.31547.

[92] C. Wu *et al.*, “Metamaterial-based integrated plasmonic absorber/emitter for solar thermo-photovoltaic systems,” *J. Opt.*, vol. 14, no. 2, 2012, doi: 10.1088/2040-8978/14/2/024005.

[93] Y. Cheng, H. Zhang, X. S. Mao, and R. Z. Gong, “Dual-band plasmonic perfect absorber based on all-metal nanostructure for refractive index sensing application,” *Mater. Lett.*, vol. 219, pp. 123–126, 2018, doi: 10.1016/j.matlet.2018.02.078.

[94] Z. Vafapour, “Polarization-Independent Perfect Optical Metamaterial Absorber as a Glucose Sensor in Food Industry Applications,” *IEEE Trans. Nanobioscience*, vol. 18, no. 4, pp. 622–627, 2019, doi: 10.1109/TNB.2019.2929802.

[95] M. Yoo, H. K. Kim, and S. Lim, “Electromagnetic-based ethanol chemical sensor using metamaterial absorber,” *Sensors Actuators, B Chem.*, vol. 222, pp. 173–180, 2016, doi: 10.1016/j.snb.2015.08.074.

[96] H. Meng, J. Wen, H. Zhao, and X. Wen, “Optimization of locally resonant acoustic metamaterials on underwater sound absorption characteristics,” *J. Sound Vib.*, vol. 331, no. 20, pp. 4406–4416, 2012, doi: 10.1016/j.jsv.2012.05.027.

[97] Y. Lin *et al.*, “Tungsten based anisotropic metamaterial as an ultra-broadband absorber,” *Opt. Mater. Express*, vol. 7, no. 2, p. 606, 2017, doi: 10.1364/ome.7.000606.

[98] C. Cao and Y. Cheng, “A broadband plasmonic light absorber based on a tungsten meander-ring-resonator in visible region,” *Appl. Phys. A Mater. Sci. Process.*, vol. 125, no. 1, p. 0, 2019, doi: 10.1007/s00339-018-2310-1.

[99] E. J. Rothwell, J. L. Frasch, S. M. Ellison, P. Chahal, and R. O. Ouedraogo, “Analysis of the Nicolson-Ross-Weir method for characterizing the electromagnetic properties of engineered materials,” *Prog. Electromagn. Res.*, vol. 157, no. October, pp. 31–47, 2016, doi: 10.2528/PIER16071706.

[100] M. I. L. Uo *et al.*, “Broadband, wide-angle, and polarization- independent metamaterial absorber for the visible regime,” *Opt. Express*, vol. 25, no. 14, pp. 16715–16724, 2017.

[101] Z. Liu *et al.*, “Automatically acquired broadband plasmonic-metamaterial black absorber during

the metallic film-formation," *ACS Appl. Mater. Interfaces*, vol. 7, no. 8, pp. 4962–4968, 2015, doi: 10.1021/acsami.5b00056.

[102] C. Li, H. Fan, Q. Dai, Z. Wei, S. Lan, and H. Liu, "Multipole resonance in arrays of diamond dielectric: A metamaterial perfect absorber in the visible regime," *Nanomaterials*, vol. 9, no. 9, 2019, doi: 10.3390/nano9091222.

[103] N. T. Q. Hoa, P. D. Tung, P. H. Lam, N. D. Dung, and N. H. Quang, "Numerical Study of an Ultrabroadband, Wide-Angle, Polarization-Insensitivity Metamaterial Absorber in the Visible Region," *J. Electron. Mater.*, vol. 47, no. 5, pp. 2634–2639, 2018, doi: 10.1007/s11664-018-6100-5.

[104] S. Butun and K. Aydin, "Structurally tunable resonant absorption bands in ultrathin broadband plasmonic absorbers," *Opt. Express*, vol. 22, no. 16, p. 19457, Aug. 2014, doi: 10.1364/oe.22.019457.

[105] H. Zhang *et al.*, "Facile Film-Nanoctahedron Assembly Route to Plasmonic Metamaterial Absorbers at Visible Frequencies," *ACS Appl. Mater. Interfaces*, vol. 11, no. 22, pp. 20241–20248, 2019, doi: 10.1021/acsami.9b01088.

[106] M. K. Hedayati *et al.*, "Design of a perfect black absorber at visible frequencies using plasmonic metamaterials," *Adv. Mater.*, vol. 23, no. 45, pp. 5410–5414, 2011, doi: 10.1002/adma.201102646.

[107] S. Cao *et al.*, "Two-dimensional subwavelength meta-nanopillar array for efficient visible light absorption," *Appl. Phys. Lett.*, vol. 102, no. 16, 2013, doi: 10.1063/1.4803046.

[108] S. Charola, S. K. Patel, K. Dalsaniya, R. Jadeja, T. K. Nguyen, and V. Dhasarathan, "Numerical investigation of wideband L-shaped metasurface based solar absorber for visible and ultraviolet region," *Phys. B Condens. Matter*, vol. 601, p. 412503, 2021, doi: 10.1016/j.physb.2020.412503.

[109] I. Hossain, M. Samsuzzaman, M. Moniruzzaman, B. B. Bais, M. S. J. Singh, and M. T. Islam, "Polarization-Independent Broadband Optical Regime Metamaterial Absorber for Solar Harvesting: A Numerical Approach," *Chinese J. Phys.*, vol. 71, no. January, pp. 699–715, 2021, doi: 10.1016/j.cjph.2021.04.007.

[110] J. Fang and B. Wang, "Optical capture capability enhancement by right-angled triangular visible absorber," *Phys. Lett. Sect. A Gen. At. Solid State Phys.*, vol. 404, p. 127404, 2021, doi: 10.1016/j.physleta.2021.127404.

**CST STUDIO SUITE 2019 Material Library